Cell Reports

Article

A bHLH interaction code controls bipotential differentiation and self-renewal in the *Drosophila* gut

Graphical abstract

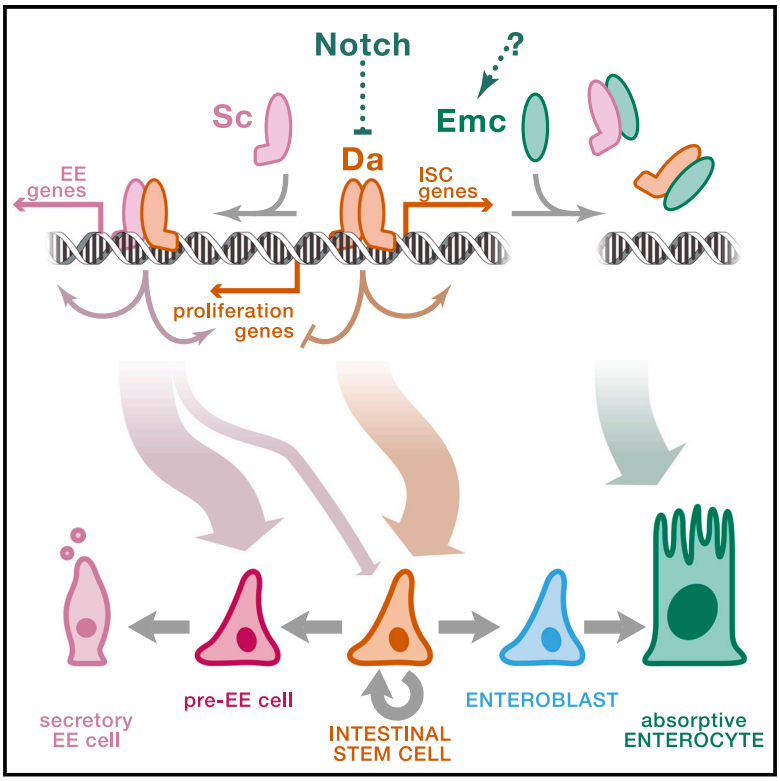

Highlights

- A network of bHLH factors regulates stemness and bipotent differentiation in the fly gut
- A careful balance between Da, Sc, and Emc determines the fate of intestinal progenitors
- Scute promotes intestinal stem cell fate as well as enteroendocrine differentiation

Authors

Aleix Puig-Barbe, Svenja Dettmann, Vinícius Dias Nirello, ..., Patrick Varga-Weisz, Jerome Korzelius, Joaquín de Navascués

Correspondence

j.denavascues@essex.ac.uk

In brief

Whether tissue stem cells balance self-renewal with multipotent differentiation through successive binary steps or a multiple-option choice is unclear. Puig-Barbe and colleagues find a dimerization network of bHLH factors in the *Drosophila* intestine that provides unified regulation to the choice between stem, absorptive, and secretory fates.

Puig-Barbe et al., 2025, Cell Reports *44*, 115398
March 25, 2025
https://doi.org/10.1016/j.celrep.2025.115398

CellPress

Cell Reports

CellPress
OPEN ACCESS

Article

A bHLH interaction code controls bipotential differentiation and self-renewal in the *Drosophila* gut

Aleix Puig-Barbe,[1] Svenja Dettmann,[2,3] Vinícius Dias Nirello,[4] Helen Moor,[5] Sina Azami,[6] Bruce A. Edgar,[2,7] Patrick Varga-Weisz,[4,5] Jerome Korzelius,[2,6,8] and Joaquín de Navascués[1,5,9,10,*]

[1]School of Biosciences, Cardiff University, The Sir Martin Evans Building, Museum Avenue, Cardiff CF10 3AX, UK
[2]DKFZ/ZMBH Alliance, University of Heidelberg, Deutsches Krebsforschungszentrum, Im Neuenheimer Feld 280, 69120 Heidelberg, Germany
[3]AbbVie Germany GmbH & Co. KG, 81 Mainzer Str., 65189 Wiesbaden, Frankfurt, Germany
[4]International Laboratory for Microbiome Host Epigenetics, Department of Genetics, Evolution, Microbiology, and Immunology, Institute of Biology, University of Campinas, Campinas, SP 13083-862, Brazil
[5]School of Life Sciences, University of Essex, Wivenhoe Park, Colchester CO4 3SQ, UK
[6]Max Planck Institute for Biology of Ageing, Joseph-Stelzmann-Straße 9B, 50931 Köln, Germany
[7]Huntsman Cancer Institute & Department of Oncological Sciences, University of Utah, Salt Lake City, UT 84112, USA
[8]School of Biosciences, University of Kent, Canterbury CT2 7NZ, UK
[9]Lead contact
[10]J.d.N. dedicates this work to the memory of Juan Modolell and Rosa María Aguilar.
*Correspondence: j.denavascues@essex.ac.uk
https://doi.org/10.1016/j.celrep.2025.115398

SUMMARY

Multipotent adult stem cells balance self-renewal with differentiation into various cell types. How this balance is regulated at the transcriptional level is poorly understood. Here, we show that a network of basic helix-loop-helix (bHLH) transcription factors controls both stemness and bipotential differentiation in the *Drosophila* adult intestine. We find that homodimers of Daughterless (Da), a homolog of mammalian E proteins, maintain self-renewal of intestinal stem cells (ISCs), antagonizing the enteroendocrine fate promoted by heterodimers of Da and Scute (Sc; homolog of ASCL). The HLH factor Extramacrochaetae (Emc; homologous to Id proteins) promotes absorptive differentiation by titrating Da and Sc. Emc prevents the committed absorptive progenitor from dedifferentiating, underscoring the plasticity of these cells. Switching physical interaction partners in this way enables the active maintenance of stemness while priming stem cells for differentiation along two alternative fates. Such regulatory logic is likely operative in other bipotent stem cell systems.

INTRODUCTION

The regulation of stem cell fate decisions hinges on transcriptional control by sequence-specific transcription factors (TFs) forming gene regulatory networks that steer cells along particular differentiation trajectories.[1–3] These trajectories are often considered a succession of binary steps regulated by cross-antagonism between TF pairs.[1,4] However, active multipotent stem cells need to decide between the maintenance of their stem identity and several options of commitment into distinct mature cell fates. To understand how multipotent stem cells make these choices, knowledge of the functional interactions between TFs is essential.[5,6]

Intestinal stem cells (ISCs) are a paradigm of multipotency in adult tissues. ISCs face a choice between self-renewal and differentiation into either the secretory or absorptive cell lineage.[7–9] The intestinal secretory lineage in *Drosophila* consists of enteroendocrine cells (EEs).[10,11] Absorptive cells are called enterocytes (ECs) and differ in morphology and function along the anterior-posterior axis of the gut.[12,13] In *Drosophila*, ISCs produce lineage-specific precursors through distinct molecular triggers. High Notch signaling induces the formation of enteroblasts (EBs), which will give rise to ECs. Expression in ISCs of the bHLH (basic helix-loop-helix) TFs Scute (Sc) and Asense (Ase), members of the *achaete-scute complex* (*AS-C*; homologs of *ASCL* mammalian genes), induces the formation of EE precursors (pre-EEs), which quickly turn into EEs.[14–16] It is not clear whether, after division of an ISC, its daughter cells first commit to differentiation before choosing a lineage (two consecutive binary decisions), are already lineage primed before they lose self-renewing ability (binary decisions in inverse order), or choose at the same time between self-renewal and two potential lineages to commit to (single triple decision).[17,18] Little is known about the molecular mechanisms that could allow a triple decision between self-renewal and bipotential differentiation.

The bHLH family of TFs control cell fate in multiple developmental contexts.[19–21] Their HLH motif mediates dimerization, while the preceding region, rich in basic amino acids, allows

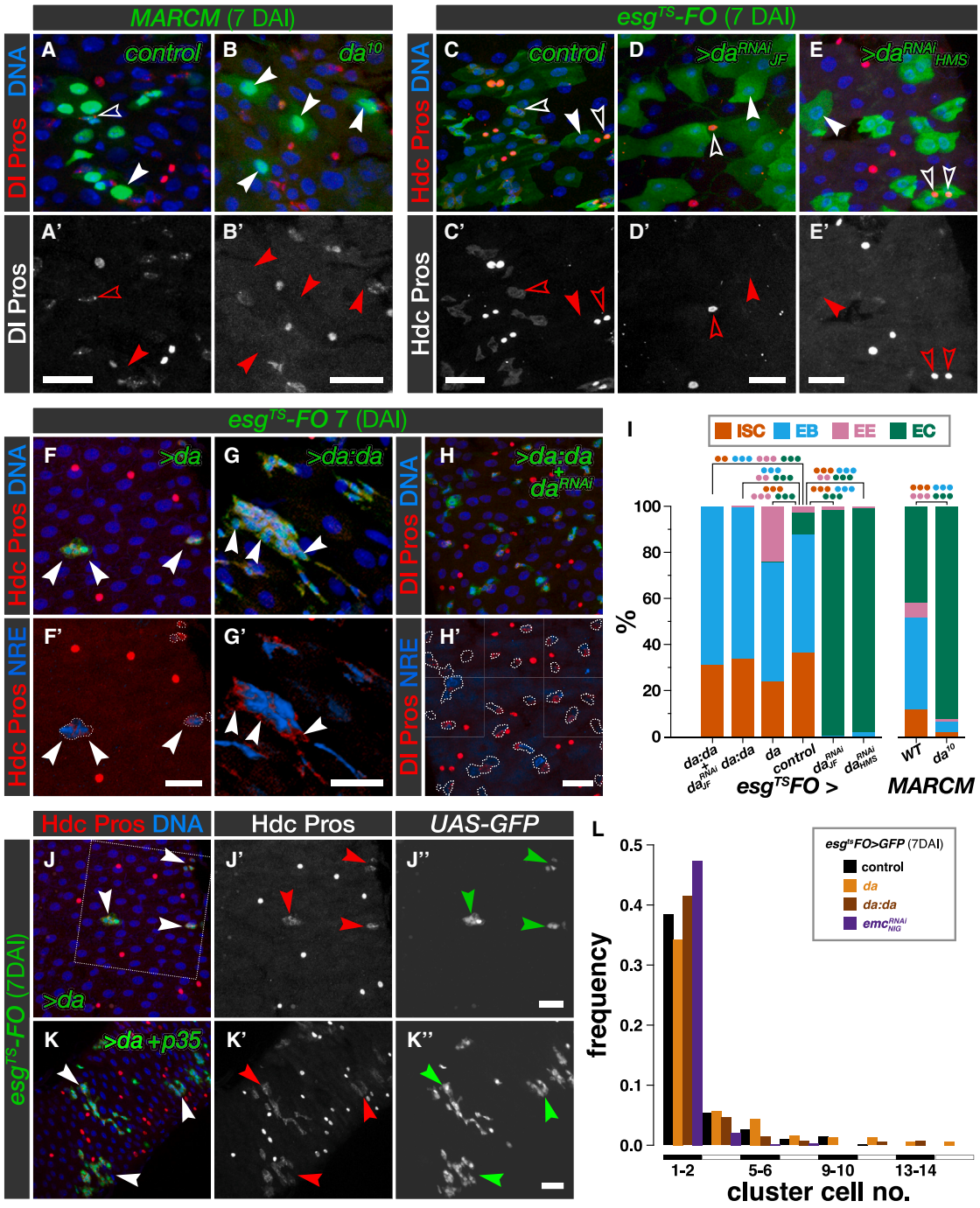

Figure 1. Da homodimers are required and sufficient to keep ISCs undifferentiated

(A and B) Cells in MARCM clones for da^{10} (B) are mostly ECs. ISCs, EBs, and EEs are dramatically reduced with respect to wild-type clones (A). (B) is reproduced in Figure 6A to aid comparison.

(C–E) Expressing da^{RNAi} with esg^{TS}-*FO* using transgenes *JF02488* (D) and *HMS01851* (E) leads to the differentiation of most cells into ECs and occasionally into EEs. Controls (C) maintain ISCs and EBs.

(A–E) Solid and empty arrowheads: ECs and ISCs or EEs, respectively.

(F and G) Overexpression of *da* (F) or *da:da* (G) with esg^{TS}-*FO* prevents formation of ECs; *da* overexpression allows EE differentiation and strongly reduces esg^{+} cell nest density. Solid arrowheads (F and G): ISCs/EBs.

(H) Overexpression of *da:da* with esg^{TS}-*FO* while depleting endogenous Da with *JF02488* interferes blocks all differentiation.

(I) Cell composition of GFP^{+} tissue and clones from (A)–(H). Some data are reproduced in Figures 7I and 7J to aid comparison.

(legend continued on next page)

DNA binding.[22] Class I bHLH factors comprise proteins such as E47, E2-2, and HEB (E proteins, encoded by *TCF3/4/12* in mammals; *daughterless* [*da*] in *Drosophila*). Class I bHLH proteins can make dimers within their class (e.g., Da:Da or E47:HEB) but can also heterodimerize with class II bHLH factors. By contrast, class II bHLH factors, such as MYOD or ASCL (MyoD and proteins encoded in the *AS-C* in *Drosophila*), usually form *trans*-activating complexes only in heterodimers with class I factors.[21] This has been specifically demonstrated for Sc and the other bHLH factors encoded in the *AS-C*.[23] By contrast, class V bHLH factors are inhibitory: they lack the stretch of basic amino acids preceding the HLH domain, rendering their heterodimers with class I and II unable to bind DNA.[21] Therefore, their mammalian members are named *Inhibitors of DNA binding* (Id proteins). Their only representative in *Drosophila* is *extra macrochaetae* (*emc*); Emc can dimerize with either Da or Sc.[24,25]

Class II bHLH factors regulate differentiation in the metazoan intestine.[9,26] In *Drosophila*, Sc and Ase can initiate EE differentiation,[14,15,27,28] while other bHLH factors maintain EE function (Dimmed, homolog of NeuroD),[29] or promote their functional diversity (Tap, homolog of Neurogenin-3).[9,26] On the other hand, Da is required for ISC maintenance, since ISCs mutant for *da* differentiate.[14] However, the interaction partners of Da to maintain stemness are not known, and how different bHLH factors dimerize to control differentiation has not been explored. Here, we identify the Da homodimer as the critical bHLH complex maintaining ISC self-renewal and find a role of Emc in titrating Da and Sc to promote absorptive differentiation. We show that Da:Da and Da:Sc dimers functionally cooperate to promote ISC fate but act antagonistically for EE differentiation. Our results reveal a network of bHLH factors that forms a three-way switch to regulate self-renewal and bipotential differentiation in the adult fly gut.

RESULTS

Da homodimers maintain stemness and prevent differentiation

We quantified the effect of *da* on differentiation in individual null da^{10} clones using Mosaic Analysis with a Repressible Cell Marker (MARCM; Figures S1A–S1B)[30] and in the entire ISC/EB population by RNAi-mediated knockdown of *da* followed by lineage tracing using the *escargot* Flip-Out approach ("esg^{TS}-*FO*"; Figure S1C).[31] Loss of *da* led to almost complete differentiation of cells into ECs, and occasionally into EEs, in da^{10} mutant clones (Figures 1A–1B, and 1I; Tables S1 and S2) and esg^{+} cells expressing da^{RNAi} (Figures 1C–1E and 1I; cell type markers as in Figure S1D). By contrast, in ISCs and EBs that overexpressed *da* with esg^{TS}-*FO*, differentiation into ECs was almost completely impaired, while EE differentiation increased (Figures 1F and 1I). Importantly, only a few esg^{+} cell nests overexpressing *da* survived, and this was rescued by co-expression of apoptosis inhibitor p35 (Figures 1J and 1K); this further reduced the overall levels of differentiation and seemed to favor the formation of EBs, a few of which became ECs (Figure S1E). While the cell composition of esg^{TS}-*FO* > *da* tissue was very different from the wild type, the size of GFP^{+} clusters expressing *da* was like that in the controls: most remained below 5 cells, and a few became considerably larger (Figure 1L).

We sought to determine the identity of the Da partners involved in preventing EC differentiation. Since Da can form homodimers to control differentiation and proliferation,[32] we overexpressed forced Da homodimers using a *da:da* tethered construct[33] with esg^{TS}-*FO* to test their capacity to block differentiation. The resulting GFP^{+} tissue comprised mostly ISCs and EBs, which distributed in clusters of similar size to the wild type (Figures 1G–1I and 1L). To test that Da homodimers were enough to maintain self-renewal without other Da-containing complexes, we expressed Da:Da while removing endogenous Da with the da^{RNAi} transgene *P{TRiP.JF02488}*, which does not target the *da:da* construct (Figure S1F). This prevented differentiation entirely (all cells were either ISCs or EBs; Figures 1H and 1I). In addition, we detected no esg^{+} cell death when the tethered *da:da* construct was overexpressed (compare Figures 1G and 1H with Figure 1J). Together, these results show that Da homodimers promote stemness; additionally, Da probably participates in another complex that induces esg^{+} cell death.

Da:Sc and Da:Da antagonize each other in secretory differentiation

Our results so far indicate that EE differentiation requires the transition from the transcriptional program of Da:Da to that of Da:Sc. This could occur through a "switch," with Da:Sc targets being epistatic over those of Da:Da, or "antagonism," whereby the relative strengths of the two programs determine the cell fate. To distinguish between these alternatives, we compared the effects of overexpressing *sc* with esg^{TS}-*FO* with those of co-expressing *da* and *sc*. Overexpression of *sc* alone leads to the induction of Pros-positive, Dl-negative and Dl/Pros-double-positive cells (Figures 2A and S2A), as expected.[14,15] This was likely mediated by Da:Sc, as the co-expression of *sc* and da^{RNAi} strongly diminished the induction of all Pros-positive cells (Figures S2A–S2C). Many of these cells exhibited the mitotic marker phospho-histone H3S10 (PH3) (Figure S2D) and were probably trapped in a pre-EE state.[15] The co-expression of *da* and *sc* greatly reduced the number of Pros-positive, Dl-negative (EE) cells and led to an increase in all Dl-positive cells (Figures 2B and 2D) while maintaining mitotic figures (Figures S2E and S2G). Since endogenous *da* is expressed weakly,[14] the overexpression of *da* and *sc* will likely produce more Da:Sc dimers than that of *sc* alone. Therefore, the suppression of the *sc* phenotype by *da*+*sc* must be due to a higher Da:Da-to-Da:Sc ratio.

(J and K) Expression of *da* with esg^{TS}-*FO* (J) results in esg^{+} cell death, with a few survivors that cannot differentiate; co-expression of *p35* (K) rescues cell death but not differentiation. (J) is a wider field of view than the tissue shown in (F). Arrows: esg^{+} Hdc^{+} ISCs/EBs. Quantified in Figure S1E.

(L) Histograms of GFP^{+} cluster sizes for esg^{TS}-*FO* driving expression of *da*, *da:da*, emc^{RNAi}, and their controls. The x axis is truncated at 16 cells, but there were larger clusters in all conditions, except emc^{RNAi}, at frequencies of 0.3% or lower.

DAI, days after induction. Scale bars: 20 μm. *p* values (binomial regression for individual cell types): ●$p < 0.05$, ●●$p < 0.01$, and ●●●$p < 0.001$. See Tables S1 and S2 for statistical details.

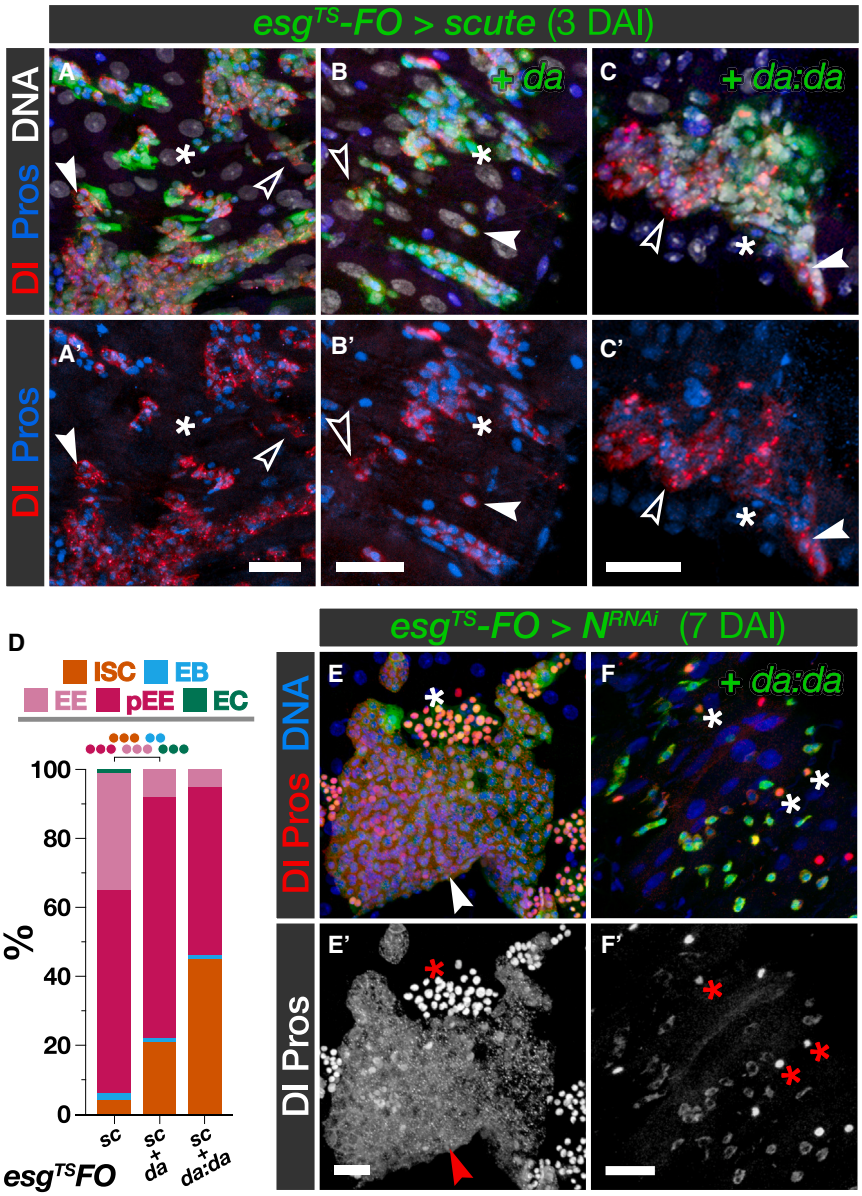

Figure 2. Da:Sc and Da:Da antagonize each other in EE differentiation

(A–C) Overexpression of *sc* with *esg*^{TS}*-FO* leads to a dramatic increase of pre-EEs and EEs but maintains a population of ISCs (A). The ISC fraction progressively increases by co-expression of *da* (B) and tethered *da:da* (C) at the cost of EE differentiation (B and C) and pre-EE formation (C).

(D) Cell composition of GFP^{+} tissue from (A)–(C).

(E and F) Knockdown of *Notch* with *esg*^{TS}*-FO* results in excess of EEs and ISCs (E); simultaneous overexpression of *da:da* rescues both phenotypes (F). Solid and empty arrowheads: pre-EEs and ISCs, respectively; asterisks: EEs. (E) is reproduced in Figure 7A to aid comparison.

DAI, days after induction. Scale bars: 20 μm. *p* values (binomial regression): ●$p<0.05$, ●●$p<0.01$, and ●●●$p<0.001$. See Tables S1 and S2 for statistical details.

This suggests antagonism between Da:Sc and Da:Da and predicts that the co-expression of tethered *da:da* and *sc* would result in even less EE differentiation, as endogenous Da available for Da:Sc dimers will be limiting. Indeed, we observed a ~2-fold increase of Dl-positive, Pros-negative cells at the expense of all Pros-positive cells, especially the Dl-negative cells (Figures 2C and 2D), with an increase in PH3^{+} cells (Figures S2F and S2G).

Loss of Notch leads to the formation of masses of Pros-positive, EE-like cells[11,14] (Figure 2E). We further tested whether Da homodimers antagonize EEs differentiation by co-expressing *da:da* and *Notch*^{RNAi} with *esg*^{TS}*-FO* and found that Pros-positive cells appeared isolated and in low numbers (Figure 2F). Thus, Da:Da and Da:Sc oppose each other in EE differentiation; intriguingly, they seem to collaborate to induce proliferation (Figures S2D–S2G) and the formation of Dl-positive, Pros-negative ISCs (Figures 2A–2D).

Both Sc and Da can impart ISC molecular and cellular properties

To understand how Da:Da and Da:Sc activate antagonistic transcriptional programs, we performed mRNA sequencing (mRNA-seq) analysis of purified *esg-Gal4 UAS-GFP* ISCs and EBs that overexpressed *da*^{RNAi}, *da*, *da:da*, or *sc*. All conditions gave distinct transcriptional signatures (Figures 3A and S3A; Table S3). Interestingly, ~1/3 of the genes downregulated upon *da*^{RNAi} expression were common to those downregulated upon *da* overexpression (Figure 3A). To explore these transcriptional signatures further, we looked at 57 cell type marker genes for ISCs, EBs, posterior midgut ECs (pECs), and EEs (Table S4) and found that both loss and gain of Da downregulate EE-specific genes (Figures 3B and S3C). This may reflect that Da homodimers prevent EE differentiation (Figures 1G–1I and 2B–2D) while Da:Sc dimers induce it[34] (Figures S2A–S2C). Consistent with this, the overexpression of *sc* strongly induced EE-specific genes; it also increased expression of the ISC-specific genes *spdo* and *Dl*. Overexpression of *da:da* or *da* alone induced ISC-specific genes (*mira* and *spdo*), while most genes expressed in the absorptive lineage (*myo31DF*, *nub/pdm1*, *αTry*, *βTry*; *E(spl)mβ-HLH*, *E(spl)m3-HLH*, and other *E(spl)* genes outside the 57-gene panel) were upregulated in *da*^{RNAi} overexpression and downregulated in the other conditions (Figures 3B, S3B, and S3C). Thus, the transcriptome analysis supports our histofluorescence observations.

To determine whether the regulated genes were potential direct targets, we scored predicted regulatory elements close

CellPress
OPEN ACCESS

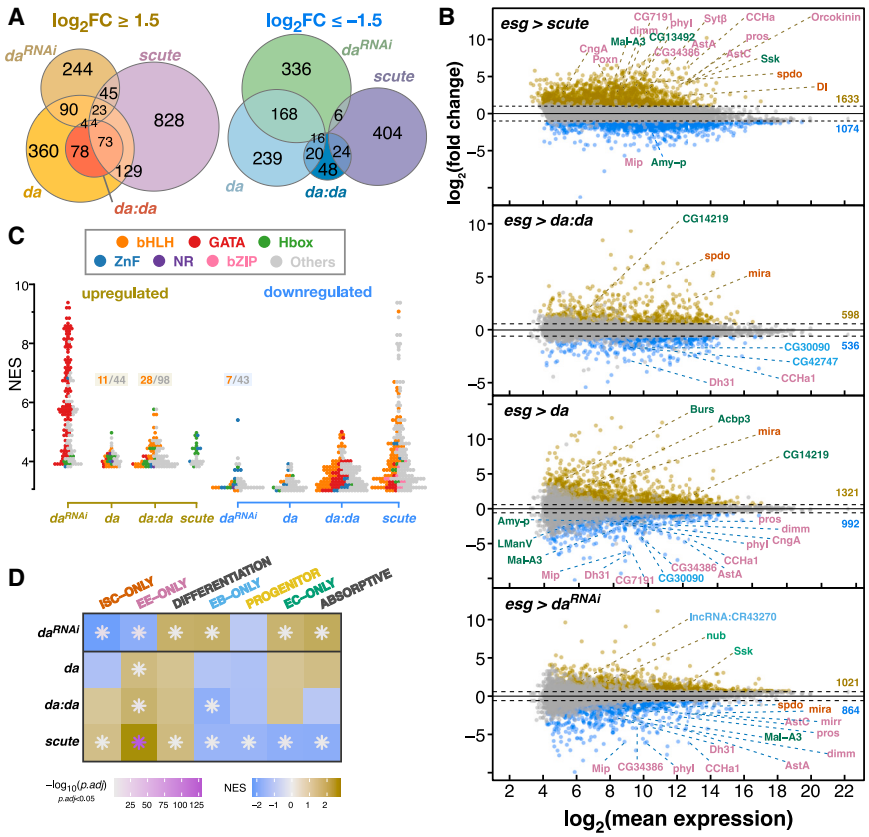

Figure 3. Da and Sc cooperate to induce the ISC transcriptional signature

(A) Euler diagram with the sizes of gene sets differentially expressed (at $|\log_2(\text{fold change})[\log_2(FC)]| \geq 1.5$) and their approximate intersections upon da^{RNAi}, *da:da*, *da*, and *sc* overexpression.

(B) MA plots for esg^{TS} > *sc*, *da:da*, *da*, and da^{RNAi}, respectively. Cell type markers are shown in colors matching Figure 1I.

(C) Normalized enrichment scores (NES) of DNA motifs found in differentially expressed genes ($|\log_2(FC)| \geq 1.5$) in the four conditions analyzed. Dots represent individual motifs and are colored by the transcription factor family that binds them. Some swarms show their bHLH motif fraction.

(D) NES heatmap for cell-type-specific gene sets; colored asterisks indicate significance.

(E and F) Enrichment plots of the transcriptional profiles induced by *sc* (E) or *da:da* (F) for ISC- and EE-specific genes. *sc* induces a clear EE signature. Some ISC genes involved in replication (*Orc2* and *Mcm2*, *-5*, *-6*, and *-7*) and mitosis (*BubR1*, *polo*, *aurB*, *sti*, and *Ndc80*) are repressed by *da:da* but activated by *sc*.

to differentially expressed genes for TF binding motifs. We found E-boxes and other bHLH binding sites over-represented in upregulated genes upon *da* or *da:da* overexpression and downregulated ones upon da^{RNAi} overexpression (Figure 3C; Table S5). We did not find enrichment in bHLH binding motifs around genes upregulated by overexpression of *sc*, which was unexpected. However, the transcriptional profile induced by *sc* corresponds mostly to differentiated EEs (Figures 3C and 3D); as *sc* is only expressed transiently to induce EE differentiation, the transcription profile we obtained may be dominated by indirect targets—not necessarily under the control of bHLH factors.

Gene set enrichment analysis[35] (GSEA) against lists of genes significantly expressed in the cell types of the midgut epithelium[36] showed that da^{RNAi} induced genes expressed in the absorptive lineage while reducing the expression of ISC- and EE-specific genes. Meanwhile, *sc* overexpression did the opposite, leading to stronger expression of ISC-specific genes than *da:da* overexpression (Figure 3D). We looked at individual genes within the regulated, ISC-specific genes. While overexpression of either *da:da* or *sc* induced regulatory genes such as *Dl* or *mira*, they had opposite effects on genes encoding factors involved in DNA replication (*Orc2*, *Mcm2*, *Mcm5*, *Mcm6*, and *Mcm7*) or mitosis (*polo*, *aurB*, *BubR1*, and *Ncd80*): these were repressed by *da:da* but induced by *sc* (Figures 3E and 3F). This highlights the capacity of *sc* to regulate key ISC-specific genes.

We also found differences in broad functional annotations between the overexpression of da^{RNAi} and that of *da*, *da:da*, or *sc*. While loss of Da induces genes involved in metabolism, biosynthesis, and energy storage and consumption, Da, Da:Da, and Sc reduced the expression signatures of these processes and favored signaling and regulatory genes (Figures S3D and S3E). We conclude that Da:Da and Da:Sc induce distinct signatures that promote the ISC and EE identities, respectively, and repress the active metabolism typical of EC function. However, Da:Da represses ISC-specific genes involved in replication and mitosis, which are upregulated by Da:Sc.

The transcriptional effects of *da:da* and *sc* overexpression on ISC-specific genes prompted us to evaluate the capacity of *sc*, *da*, or *da:da* to impose ISC properties on more differentiated cells. We targeted EBs, which are lineage committed and postmitotic, using the driver NRE^{TS}-*FO* (Figure S4A). Wild-type EBs labeled with NRE^{TS}-*FO* either remained undifferentiated or became ECs; negligible numbers expressed Dl or Pros (Figures 4A and 4E). Driving the expression of *sc*, *da*, or *da:da* with NRE^{TS}-*FO*

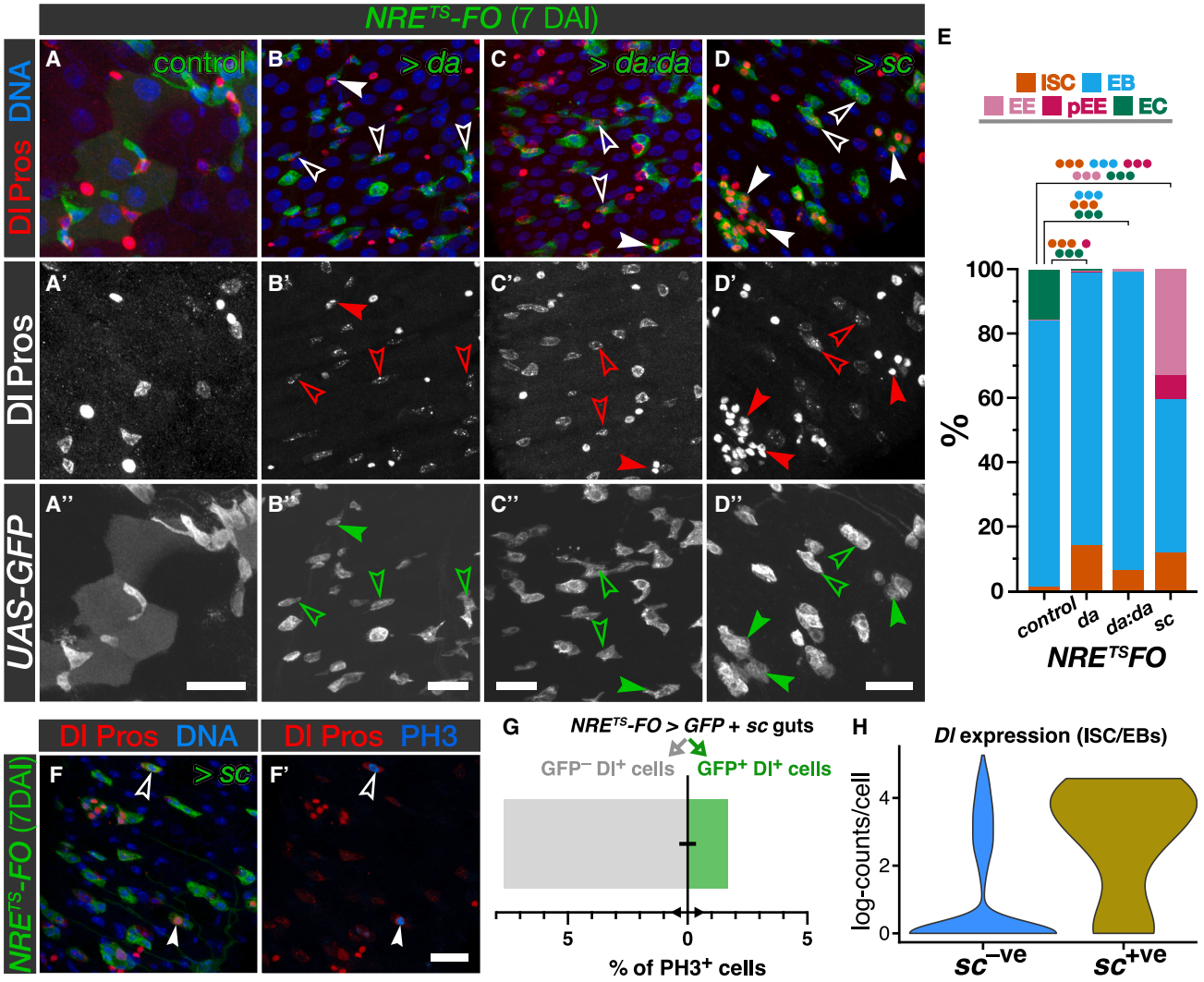

Figure 4. Da:Sc and Da:Da can impose ISC properties on EBs

(A–D) Expression of *da* (B), *da:da* (C), or *sc* (D) with *NRE^{TS}-FO* (see Figure S4A) blocks normal EC differentiation (compare with A) and promotes re-expression of Dl (empty arrowheads) and EE differentiation (solid arrowheads). EB-derived EEs occur occasionally upon *da* or *da:da* overexpression but are very frequent upon *sc* overexpression, which also induces the formation of pre-EEs.

(E) Cell composition of GFP$^+$ tissue from (A)–(D).

(F) Overexpression of *sc* with *NRE^{TS}-FO* shows both Dl$^+$ and Pros$^+$ cells (empty and solid arrowheads, respectively) undergoing mitosis (phospho-H3$^+$).

(G) Proportions of mitotic Dl$^+$ cells (Pros$^+$ or Pros−) within and out of the population of cells co-expressing *GFP* and *sc* in *NRE^{TS}-FO>GFP + sc* intestines ($n = 303$ cells).

(H) Expression (in logcounts) of *Dl* found in ISCs/EBs by scRNA-seq (see Figure S5I), segregated by the expression of *scute* (zero vs. non-zero counts).

DAI, days after induction. Scale bars: 20 μm. *p* values (binomial regression): ●$p < 0.05$, ●●$p < 0.01$, and ●●●$p < 0.001$. See Tables S1 and S2 for statistical details.

abolished EC differentiation and led to a significant increase of Dl-positive cells (Figures 4B–4E). *sc* overexpression in EBs also induced many pre-EEs and EEs (Figures 4D and 4E). This suggested that Da, Da:Da, and Sc could force EBs to revert to the ISC fate and also, in the case of Sc, to the secretory lineage. Incidentally, while *da* overexpression in ISCs/EBs induced cell death (Figures 1J–1K), its overexpression in EBs only with *NRE^{TS}-FO* did not. We evaluated whether these induced Dl-positive cells could, like ISCs, undergo mitosis. We found mitotic (PH3-positive) cells within the EB-derived Dl-positive cells overexpressing *sc*; their proportion was of the same order as the mitotic, endogenous ISCs within the same tissue (2% vs. 7%; Figures 4F and 4G). To assess whether *sc* may be promoting ISC properties in normal homeostasis, we analyzed published single-cell RNA-seq (scRNA-seq) datasets[37,38] (Figure S4B) and found that cells classified as ISC/EBs that expressed *sc* had, on average, much higher levels of *Dl* (Figure 4H), suggesting that *sc*, apart from inducing EE differentiation, normally promotes the expression of ISC features.

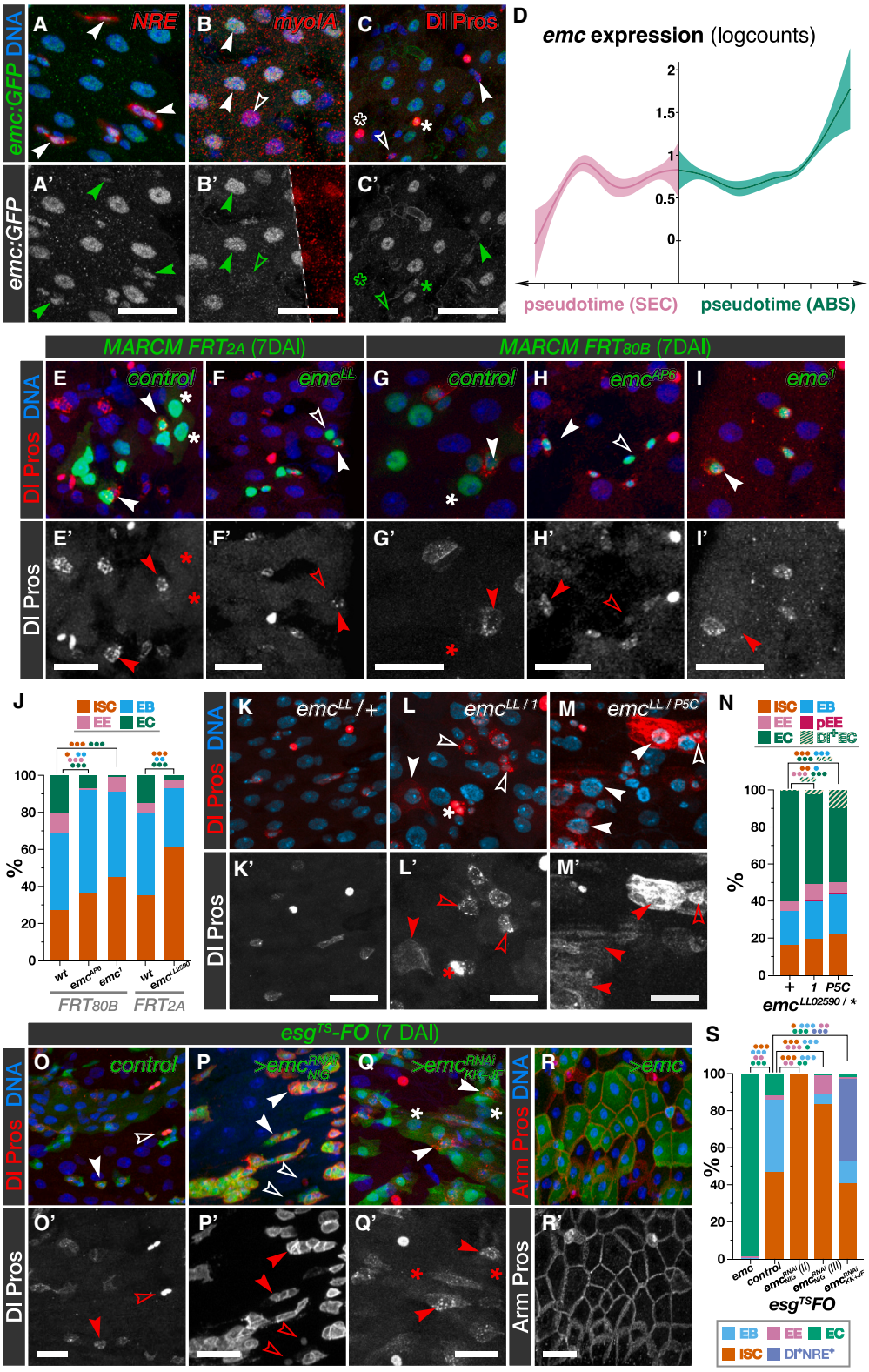

(legend on next page)

Emc promotes EC differentiation by titrating Da

Da and Sc functions are often antagonized through direct binding and titration by the HLH class V factor Emc, which prompted us to test *emc* function in intestinal homeostasis. Using the protein-trap line $emc^{CPTI002740}$,[39] we found that *emc* was expressed in all cell types of the adult gut but predominantly in EBs and ECs (Figures 5A–5C). scRNA-seq data[37,38] show that *emc* expression is mainly in EBs and ECs of the posterior midgut, with cell type distributions similar to *bona fide* markers of pECs and EBs (Figures S5A–S5H). Consistent with this, *emc* expression decreases along the transcriptional trajectory from ISC/EB to EE and increases in the ISC/EB-to-pEC trajectory (Figures 5D and S5I). Note also how ISCs/EBs expressing sc^{+} (and higher *Dl*) are located, within the ISC/EB cluster, at the beginning of the differentiation trajectories (Figures S5I and 4H). MARCM clones mutant for $emc^{LL02590}$ (Figure S5J) had fewer differentiated cells and were enriched in Dl-positive ISCs (Figures 5E–5F and 5J). Clones for alleles emc^{1} and emc^{AP6} (Figure S5J) showed similar enrichment in Dl-positive ISCs compared to wild-type clones (Figures 5G–5J). Hypomorphic viable $emc^{LL02590}/emc^{1}$ and $emc^{LL02590}/emc^{P5C}$ heterozygotes (Figure S5J) showed an increase in ISCs/EBs at the expense of ECs, accompanied by higher levels of Dl in ISCs and its ectopic expression in ECs, compared to control $emc^{LL02590}$/+ guts (Figures 5K–5N). Knockdown of *emc* with esg^{TS}-*FO* phenocopied the overexpression of *da*: ISCs/EBs gave rise to labeled clusters of similar size to the controls (Figure 1L) where differentiation was severely impaired (Figures 5O–5Q and 5S). The strength of the effect on differentiation in the emc^{RNAi} transgenes correlated with their efficacy in depleting Emc protein and inducing "*extra macrochaetae*" phenotypes (Figures S5K–S5R). The strongest emc^{RNAi} transgene (*NIG-1007R*) induced, as with *da* overexpression, the loss of many esg^{+} cell nests by apoptosis. As in the case of *da* overexpression, co-expression of *p35* and emc^{RNAi} prevented ISC/EB death (Figures S6A and S6B), displayed reduced differentiation with respect to controls, and contained more EBs than emc^{RNAi} alone (Figure S6A–S6C). We conclude that *emc* is necessary for EC differentiation and the survival of ISCs and EBs. Overexpression of *emc* with esg^{TS}-*FO* resulted in all ISCs/EBs differentiating into ECs (Figures 5R and 5S), as expected.[40] Therefore, Emc is both necessary and sufficient to direct absorptive differentiation.

If Emc promoted EC differentiation by titrating Da and Sc, then *emc* function should depend on *da*. We tested this by generating MARCM clones mutant for *da* and expressing emc^{RNAi} or mutant for *emc* and expressing da^{RNAi}. Both conditions led to EC differentiation like in da^{10} clones (compare Figures 6A–6C with Figure 6D). Considering our previous results where *sc* promoted ISC characteristics (Figures 3 and 4) and that ISCs express Sc,[15,41] we tested whether the effects of *emc* loss depended on *sc* or any other member of the *AS-C*. We induced MARCM clones for $Df(1)sc^{B57}$ (a deletion of the *AS-C*)[42] expressing emc^{RNAi} and compared them with clones that only expressed emc^{RNAi}. Differentiation was impaired in both conditions (Figures 6F and 6G), but Dl expression was 4-fold lower in the absence of the *AS-C* (Figure 6H). We conclude that Emc promotes EC differentiation and dampens Dl expression by preventing the formation of Da:Da and Da:Sc dimers, respectively.

emc is required for the commitment of EBs

The requirement of *emc* for differentiation prompted us to investigate whether it was necessary to maintain the commitment of EBs as absorptive progenitors. We used the EB-specific driver NRE^{TS}-*Gal4*, which never co-expresses with Dl in the wild type, to express emc^{RNAi}. This led to Dl expression in NRE^{+} cells (Figures S6C and S6D), suggesting that *emc*-depleted EBs may revert to ISCs. We verified this with NRE^{TS}-*FO* driving emc^{RNAi} expression and observed that *emc*-depleted EBs give rise to Dl-positive cells (Figures 6I and 6J) that undergo mitosis (PH3 positive) at a similar frequency to neighboring normal ISCs (Figures 6I and K). This suggests that *emc* is necessary for the commitment of EBs.

Notch and emc converge independently on Da to regulate ISC fate

Notch signaling is key for ISC differentiation and absorptive fate acquisition.[10,11] We found that simultaneous knockdown of *N*

Figure 5. *emc* is necessary and sufficient to induce EC differentiation

(A–C) Expression of Emc-GFP in the homozygous viable protein-trap insertion $emc^{CPTI002740}$. Emc is expressed in EBs (*NRE-lacZ*$^{+}$, arrowheads) (A) and some ECs (*myoIA-lacZ*$^{+}$, solid arrowheads) but not all (empty arrowheads) (B). Some ISCs (Dl^{+}, solid arrowheads) and EEs (Pros^{+}, solid asterisks) express Emc but many do not (empty arrowheads and asterisks) (C).

(D) *emc* expression along the pseudotime trajectories from ISCs/EBs into EEs and ECs (Figure S5I) decreases toward the secretory fate and increases toward the absorptive one. The continuous line represents mean values; shading represents its standard error.

(E–I) Cells in MARCM clones for $emc^{LL02590}$ (F), emc^{AP6} (H), and emc^{1} (I) are enriched in ISCs (solid arrowheads) and EBs (empty arrowheads) compared to controls (E and G). FRT_{80B} and FRT_{2A} are two independent insertions for inducing MARCM clones in chromosomal arm 3L.

(J) Cell composition of clones from (E)–(I).

(K–M) Midguts of viable hypomorphic mutants $emc^{LL02590/1}$ (L) and $emc^{LL02590/P5C}$ (M) contain more ISCs, pre-EEs (L, asterisk), and EEs and less ECs than heterozygous controls (K). In these mutants, Dl expression is elevated in some ISCs (L and M, empty arrowheads) and ectopic in some ECs (L and M, solid arrowheads).

(N) Cell composition in genotypes from (K)–(M).

(O–Q) Expressing emc^{RNAi} with esg^{TS}-*FO* using transgenes *NIG-1007R* (P) or *KK108316* and *JF02300* together (Q) increases the proportion of Dl^{+} cells (solid arrowheads) and EEs (empty arrowheads) and reduces that of ECs (asterisks) compared to controls (O). *KK108316* and *JF02300* together produced Dl^{+}, *NRE-lacZ*$^{+}$ cells, possibly dedifferentiating EBs (see Figures 6I and 6J) or cells with mixed ISC/EB identity or marker expression. emc^{RNAi} also increases Dl expression (P and Q), especially with *NIG-1007R* (P).

(R) Overexpression of *emc* with esg^{TS}-*FO* forces differentiation into ECs.

(S) Cell composition in genotypes from (O)–(R).

DAI, days after induction. Scale bars: 20 μm. *p* values (binomial regression): ●$p < 0.05$, ●●$p < 0.01$, and ●●●$p < 0.001$. See Tables S1 and S2 for statistical details. (F), (P), and (R) are reproduced in Figures 6D, S7G, and S7C, respectively, to aid comparison.

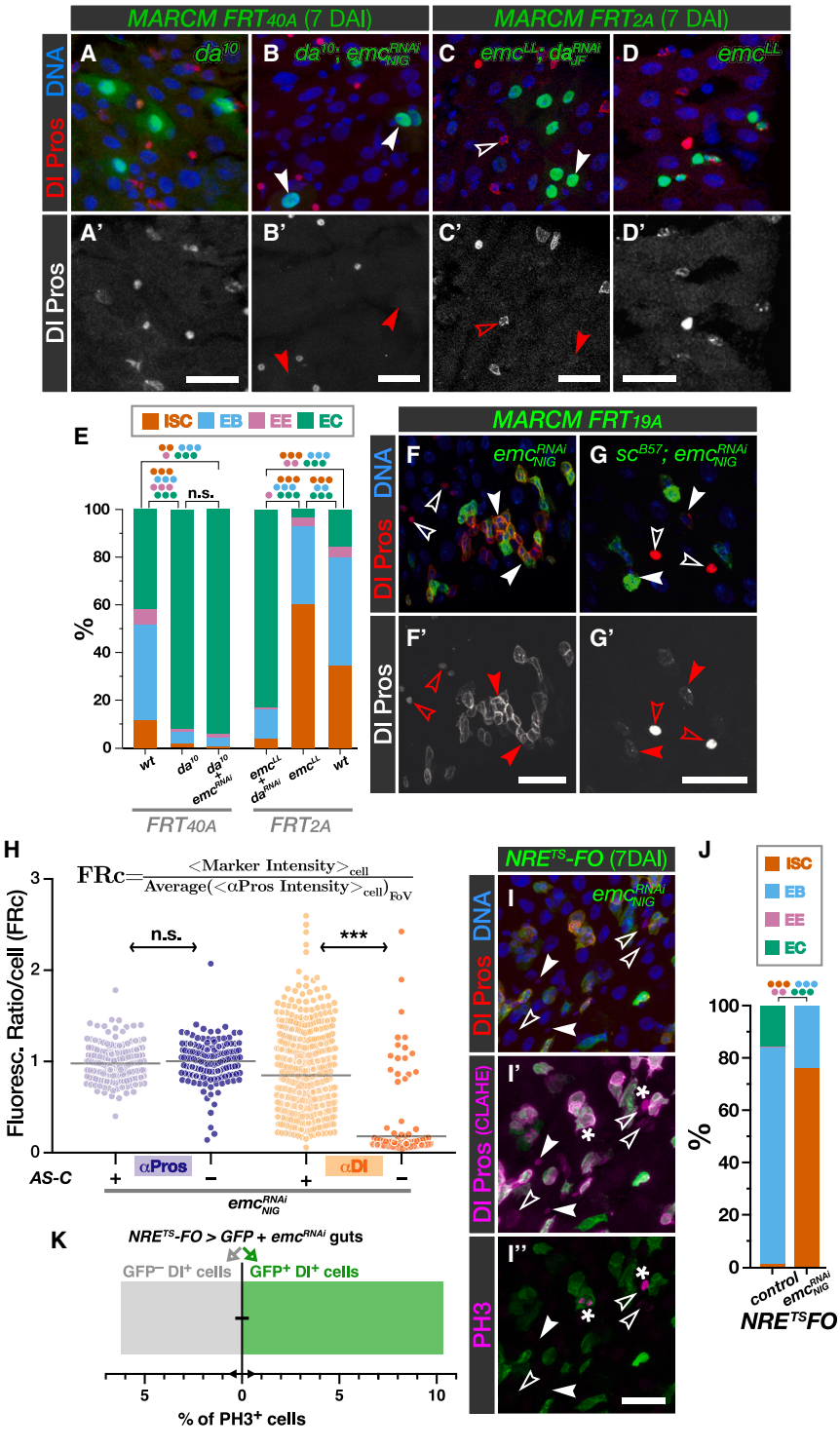

Figure 6. *emc* antagonizes *da* and *sc* in the intestine and keeps EBs committed

(A–D) *da* is epistatic over *emc*. Solid arrowheads: ECs; empty arrowheads: ISCs. Cells in MARCM clones that are mutant for da^{10} and express emc^{RNAi} *NIG-1007R* (B) mostly differentiate into ECs, like in da^{10} clones (A). Cells in MARCM clones that are mutant for $emc^{LL02590}$ and express da^{RNAi} *JF02488* (C) also differentiate into ECs, suppressing the reduced differentiation of $emc^{LL02590}$ cells (D).

(E) Cell composition of clones from (A)–(D) and Figure 1I. Note that da^{10} is statistically indistinguishable from da^{10}; emc^{RNAi}.

(F and G) Emc antagonizes Sc in inducing *Dl*. Loss of the *achaete-scute complex* (*AS-C*) using deficiency $Df(1)sc^{B57}$ reduces the elevated Dl expression observed with emc^{RNAi} (G, compare with F).

(H) Quantification of relative levels (fluorescence ratio) of Pros and Dl per cell, normalized by the average of Pros per field of view (FoV; see the equation on top of the figure axes and STAR Methods), for 210, 146, 718, and 210 cells per group from left to right. Horizontal lines are averages per category. *p* values (Mann-Whitney test): ***$p < 0.001$ and n.s. $p \geq 0.05$.

(I–K) Expressing emc^{RNAi} *NIG-1007R* with NRE^{TS}-*FO* prevents EB differentiation and activates Dl expression (I′, solid arrowheads) at higher levels than extant ISCs (arrowheads; extant ISCs are detectable after contrast-limited adaptive histogram equalization [CLAHE]). These cells are mitotic (I′′, phospho-histone H3, asterisks) at levels similar to extant ISCs (K) and have presumably reverted into ISCs (quantified in J).

Scale bars: 20 μm. *p* values (binomial regression in stacked bars): ●$p<0.05$, ●●$p<0.01$, ●●●$p<0.001$, and n.s. ≥ 0.05. See Tables S1 and S2 for statistical details. (A) and (D) are reproduced from Figures 1B and 5F, respectively, to aid comparison.

and *da* with esg^{TS}-*FO* prevented the tumorous expansion of Dl-positive and Pros-positive cells typically found with N^{RNAi} alone[10,43] and forced most cells to differentiate as ECs (Figures 7A, 7B, and 7D). This extent of EC differentiation in the absence of Notch has not been seen before[10,11,14,34,44,45] and strongly suggests that the Notch pathway could be regulating Da. To activate or prevent Notch signaling, we used esg^{TS}-*FO* to knock down or overexpress Hairless (H), the specific co-repressor for the transcriptional targets of Notch.[46] Overexpression of *H* with esg^{TS}-*FO* resulted in the expansion of Dl-positive cells and EE differentiation (Figures 7E and 7I).[14] Simultaneously knocking down *da* prevented ISC and EE expansion and induced high levels of EC differentiation (compare Figures 7F and 7I with Figure 7D). Conversely, the expression of H^{RNAi} with esg^{TS}-*FO* leads to an increase in EC differentiation and the expression of *NRE-lacZ* in all diploid cells (Figures 7G and 7I).[14] The co-expression of *da:da* with H^{RNAi} prevents all EC differentiation, with all esg^{+} cells becoming *NRE-lacZ*$^{+}$ (Figures 7H and 7I). Thus, *da* is epistatic over Notch signaling, suggesting that at least part of the function of Notch to induce differentiation is to repress Da. Next,

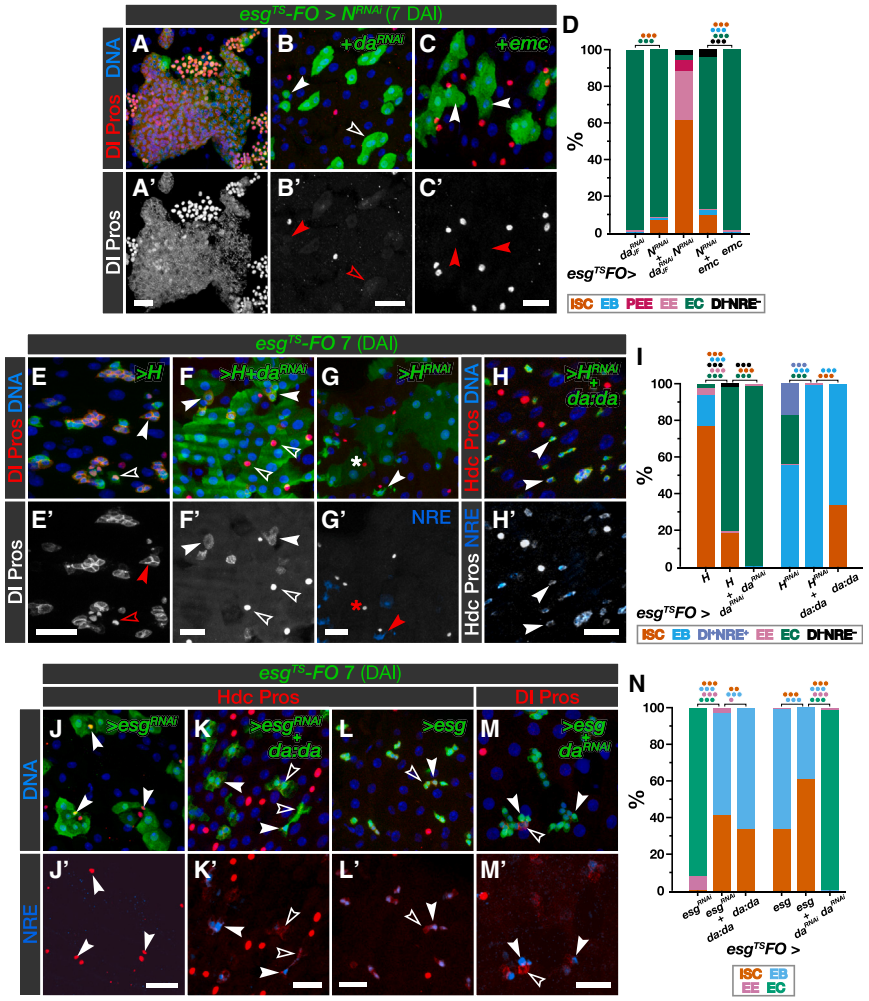

Figure 7. *da* is epistatic to Notch signaling and acts in parallel with *esg*

(A–C) Expressing N^{RNAi} together with da^{RNAi} (B) or *emc* (C) using esg^{TS}*-FO* leads to EC differentiation, abolishing the tumorous expansion of Dl^+ and $Pros^+$ cells with N^{RNAi} alone (A). Solid arrowheads: polyploid ECs; empty arrowheads: Dl^- diploid cells (EBs or early ECs). (A) is reproduced from Figure 2E to aid comparison.

(D) Cell composition of GFP^+ tissue from (A)–(C); data from Figures 1I and S5 are replicated here to aid comparison.

(E and F) Expressing *H* with esg^{TS}*-FO* (E) blocks EC differentiation and leads to accumulation of ISCs. This is rescued by simultaneous expression of da^{RNAi} (F). Solid arrowheads: ISCs; empty arrowheads: EEs.

(G and H) Expressing H^{RNAi} with esg^{TS}*-FO* (G) induces EC differentiation, some EE differentiation (asterisk), and the expression of the *NRE-lacZ* reporter in all esg^+ cells (solid arrowhead). Simultaneous expression of *da:da* (H) blocks the formation of ECs, as in esg^{TS}*-FO>da:da* alone, and all cells become *NRE-lacZ*$^+$ (solid arrowheads).

(I) Cell composition of GFP^+ tissue from (E)–(H); data from Figure 1I are replicated here to aid comparison.

(J and K) Knockdown of *esg* with esg^{TS}*-FO* (J) induces differentiation of all cells into ECs and EEs (solid arrowheads); this is prevented by simultaneous expression of *da:da* (K), which blocks differentiation of ISCs (empty arrowheads) and EBs (solid arrowheads) to the same levels as in esg^{TS}*-FO>da:da* alone (see N).

(L and M) Expression of *esg* with esg^{TS}*-FO* (L) blocks differentiation regardless of whether *da* is simultaneously knocked down (M). Empty arrowheads: ISCs; solid arrowheads: EBs.

(N) Cell composition of GFP^+ tissue from (J)–(M); data from Figure 1I are replicated here to aid comparison.

p values (binomial regression for individual cell types): ●$p < 0.05$, ●●$p < 0.01$, and ●●●$p < 0.001$. See Tables S1 and S2 for statistical details. DAI, days after induction. Scale bars: 20 μm. (E) and (G) are reproduced in Figures S7A and S7E, respectively, to aid comparison.

we asked whether this function was exerted through the induction of *emc*.

emc transcription is regulated by Notch signaling in multiple tissues,[47–51] and we found that co-expressing *emc* and N^{RNAi} with esg^{TS}*-FO* leads to EC differentiation (Figures 7C and 7D). Therefore, Notch could be inducing EC differentiation by activating Emc, which in turn would titrate Da. *emc* expression induces EC differentiation rapidly,[52] so these esg^{TS}*-FO>emc+* N^{RNAi} ECs could have differentiated before N protein was depleted. To inhibit Notch signaling faster, we co-expressed *H* with *emc* using esg^{TS}*-FO*. This led to an increase in EC differentiation compared to expression of *H* alone but far from the near-complete EC differentiation observed when only expressing *emc* (Figures S7A–S7D) or expressing *H with* da^{RNAi} (compare with Figures 7F and 7I). This suggests that Emc can induce EC differentiation in the absence of Notch signaling but not efficiently. Moreover, expressing H^{RNAi} and emc^{RNAi} with esg^{TS}*-FO* did not prevent the excess EC differentiation observed upon expression of H^{RNAi} alone; this contrasts with the capacity of emc^{RNAi} to block differentiation entirely (Figures S7D–S7G). Therefore, Emc is dispensable for Notch to induce EC differentiation. Moreover, clonal expression of the Notch intracellular domain does not induce *emc* expression in any cell type of the midgut epithelium (Figure S7H). We conclude that *emc* and Notch signaling act independently to promote the absorptive fate.

Da:Da and Esg block differentiation independently

Esg, a TF of the Snail family, regulates ISCs by preventing ISC/EB differentiation.[44,45] As Da:Da dimers have the same capacity, we considered whether Esg and Da act together to maintain stemness. Expression of esg^{RNAi} with esg^{TS}*-FO* led to differentiation into ECs and EEs (Figures 7J and 7N) as expected.[34,44,45] The simultaneous overexpression of esg^{RNAi} and *da:da* blocked EC differentiation and significantly reduced the formation of EEs (Figures 7K and N). In turn, the expression of *esg* with esg^{TS}*-FO* blocked differentiation, irrespective of whether da^{RNAi} was also expressed (Figures 7L–7N). This independence seems mirrored in their downregulated gene sets: almost half the Esg repression

targets[44] overlap with genes downregulated by misexpression of *da* or *da:da* or upregulated by misexpression of da^{RNAi}, including genes essential for EC function like *nub/pdm1*, *ssk*, and *Tsp2A* (Figure S7I). Finally, we observed that the expression of neither *da* nor *esg* was affected by the overexpression of the other (Figures S7J and S7K). We conclude that *da* and *esg* contribute to stemness independently of each other.

DISCUSSION

We demonstrate a central role for a bHLH factor code in the acquisition and maintenance of three alternative cell fates in the adult *Drosophila* intestine. Class I homodimers (Da:Da) maintain the progenitor state of ISCs/EB, with changes in dimerization partners governing the fate transitions. Sequestration of Da with class V HLH factor Emc into Da:Emc dimers incapable of DNA binding induces progenitor cells to acquire the absorptive fate, while the formation of Da:Sc dimers by binding of Da with class II bHLH Sc initiates EE differentiation (Figures 2 and S2).[14,16] Moreover, Emc is required in EBs to maintain their committed state, while low levels of Sc boost aspects of the ISC transcriptional state.

Three cell fates regulated by a dimerization network

Networks involving class I, II, and V bHLH factors regulate the development of the *Drosophila* retina[53] and peripheral nervous system.[25,54,55] However, in these cases, the choice is between only two alternative fates (neural vs. epidermal), with Da homodimers promoting the same fate as heterodimers between Da and a class II bHLH proneural factor.[53,55,56] By contrast, in the adult midgut, Da:Da and Da:Sc promote distinct fates (progenitor and secretory, respectively) through distinct transcriptional programs, while Emc titrates both dimers to allow EC differentiation. This integrated mechanism suggests that the balance between ISC self-renewal and absorptive or secretory differentiation rests on a triple choice rather than two consecutive binary decisions. An equivalent network could operate in similar stem cell systems, and it is tempting to speculate on this possibility in the mammalian intestine, where the relevant factors (mouse *da* homologs *E2a* and *Heb*, *emc* homolog *Id1*, and *sc* homolog *Ascl1*) are expressed in the crypts of Lieberkühn and have roles in fate determination.[57–59]

A balance of factors regulates ISC fate

We refer to the Da/Emc/Sc network as a bHLH code due to its modularity, but it does not behave as a Boolean switch; the relative abundance of the different components seems critical. Da, the centerpiece of the network, forms homodimers that maintain stemness and prevent EC and EE differentiation (Figures 1 and 2), but it is also an essential partner for Sc in EE differentiation (Figure S2). The activity of Da homodimers in promoting stemness is also nuanced, as, in parallel to activating some ISC genes and repressing some EE/EC ones, Da:Da downregulates proliferation effector proteins, in agreement with its previously reported anti-proliferative activity.[60] Strikingly, an excess of Da monomers (whether induced directly by overexpression or indirectly by loss of Emc) promotes apoptosis (Figures 1 and S6), while the excess of Sc or tethered Da:Da does not. It follows that Da also participates in an apoptosis-promoting complex yet to be identified. By contrast, the activity of Emc is determinant but not intrinsically instructive: through titration of Da and Sc, cells have to differentiate but lack the capacity to initiate EE differentiation, so they differentiate into ECs by default. However, Emc loss in EBs induces expression of ISC features, possibly through the increased activity of Sc (Figure 6), and prevents Da from inducing apoptosis of ISC/EBs (Figure S6). This makes Emc also an essential factor in maintaining the progenitor population. Sc, which is normally expressed at low levels in ISCs,[15,41] triggers EE differentiation when expressed over a threshold.[14,15,27] We find that Sc boosts the expression of essential ISC genes, such as Dl or those involved in proliferation. Moreover, Sc seems to induce fate reversal in EBs. Therefore, Sc also boosts the ISC function, which sits well with the role of its homolog *Acsl2* in maintaining mammalian ISCs.[57]

We conclude that a dynamic balance of Da, Emc, and Sc is required for homeostasis and that this bHLH code is not composed of "master" but rather contextual regulators. This pushes the question toward the regulation of their protein concentrations and/or functions across intestinal cell types and over time. The specific role of Notch signaling in regulating Da and the identity of *emc* regulators is bound to be informative.

In line with this view, another essential regulator of ISC fate, Esg, operates in parallel to the bHLH network. Excess of either Esg or Da can compensate for the absence of the other to keep ISCs/EBs undifferentiated, suggesting that at physiological levels, when either is essential for stemness (Figure 1),[44] they have some additive effect. This may be reflected in the significant overlap of their downregulated genes (Figure 7), which includes the EC fate inducer *nub/pdm1*. On the other hand, Esg seems to have a more specific role than Da:Da in preventing EE differentiation and lacks its anti-proliferative activity,[44,45] suggesting that they also govern non-shared aspects of ISC identity and function. These non-redundant layers of regulation likely allow fine-tuning of the ISC function.

Multiple factors maintain EB commitment

Notch signaling induces the formation of EBs,[10,11] which, under normal conditions, give rise to mature ECs without further division (Figure 4).[16,61,62] EBs are relatively long lived,[63] and though they are recognized by expression of the *NRE*, once formed, they do not need Notch to maintain their commitment.[64] However, we found that they require Emc, as its depletion in EBs gave rise to Dl-expressing proliferative cells—likely a reversal of fate toward ISCs. Qualitatively similar effects resulted from misexpressing *da*, *da:da*, or *sc* in EBs. We interpret that combined baseline levels of Da and Sc in EBs may lead them to revert their fate into ISCs if not titrated by Emc. EB-to-ISC reversion is also prevented by TF Sox21a[65] and the global co-repressor Groucho.[66] EB-to-EE *trans*-differentiation has also been observed when either Ttk69 or Klu was depleted or Phyllopod overexpressed in EBs.[61,62,67] These observations underscore the plasticity of the EB and resemble the behavior of EC precursors in the mammalian intestine, which can dedifferentiate and repopulate the intestinal crypt during regeneration.[68]

Limitations of the study

Our interpretation of the functional relationships between Da, Sc, and Emc are based on misexpression tools with no control over resulting stoichiometry. Future studies should address this limitation with newly developed tools with more precise control.[69–71] Our analysis of *emc* function involved the emc^{RNAi} transgene *NIG-1007R*, which is far more effective at depleting Emc than either *KK108316* or *JF02300* or both combined (Figure S5). Several *emc* loss-of-function conditions affecting large amounts of tissue induce increased Dl expression (Figure 5), but with *NIG-1007R*, this effect is much higher and not observed in MARCM *emc* null clones. This may point to non-cell-autonomous, suppressing effects on Dl expression that are only inactivated when the whole tissue or the whole progenitor population is affected. We are confident that *NIG-1007R* elicits genuine *emc* loss phenotypes because: the strength of the increase in Dl levels correlates with the strength of the emc^{RNAi} transgenes (Figures 5 and S6); *NIG-1007R* phenocopies the overexpression of *da*, including the induction of apoptosis (which *KK108316* and *JF02300* cannot recapitulate; Figures 1, 5, and S5); and we can fully rescue the increase in Dl expression induced by *NIG-1007R* by simultaneous loss of *sc* (Figure 6). While our tenet does not hinge on this observation, it deserves future attention.

RESOURCE AVAILABILITY

Lead contact

Further information and requests for resources and reagents should be directed to and will be fulfilled by the lead contact, Joaquín de Navascués (j.denavascues@essex.ac.uk).

Materials availability

Drosophila strains generated in this study are available upon request. Requests for *Drosophila* strains should be directed to and will be fulfilled by the lead contact.

Data and code availability

- RNA-seq data have been deposited at GEO and are publicly available as of June 7, 2023. The accession number is in the key resources table. Microscopy data reported in this paper will be shared by the lead contact upon request.
- scRNA-seq data were generated by Hung et al.[37] and Li et al.[38] and obtained from GEO and Array Express, respectively. The accession numbers are in the key resources table.
- This paper does not report original code.
- Any additional information required to reanalyze the data reported in this work paper is available from the lead contact upon request.

ACKNOWLEDGMENTS

We thank the anonymous reviewers for helpful suggestions; Nicholas Baker, Allison Bardin, Antonio Baonza, Sonsoles Campuzano, Sangbin Park, Mike Taylor, Shinya Yamamoto, Alfonso Martínez-Arias, the Bloomington *Drosophila* Stock Center, the Vienna *Drosophila* Resource Center, the *Drosophila* Genetics Resource Center (Kyoto), and the National Institute of Genetics (Japan) for providing fly stocks; the Developmental Studies Hybridoma Bank (University of Iowa) for supplying antibodies; and Juan Modolell, Sonsoles Campuzano, Catherine Hogan, Fernando dos Anjos-Afonso, Florian Siebzehnrubl, Terrence Trinca, Sonia López de Quinto, Helen White-Cooper, Mike Taylor, and Wynand van der Goers van Naters for critical comments on the manuscript and useful discussions. We acknowledge the data analysis team of the College of Biomedical and Life Sciences of Cardiff University and the FACS and Imaging Core Facility at the Max Planck Institute for Biology of Aging for technical assistance. This work was supported by funding from Cardiff University to J.d.N. and A.P.-B., the University of Essex and NC3Rs SKT grant NC/W001047/1 to P.V.-W. and J.d.N., DFG grant KO5594/1-1 and an EMBO Long-Term Fellowship to J.K., Fundação de Amparo à Pesquisa do Estado de São Paulo (FAPESP) fellowship #2021/00393-9 to V.D.N., FAPESP São Paulo Excellence Chair #2019/16113-5 to P.V.-W., and ERC Advanced Grant no. 268515 to B.A.E.

AUTHOR CONTRIBUTIONS

Conceptualization, J.d.N.; data curation, J.d.N., A.P.-B., and J.K.; formal analysis, J.d.N., A.P.-B., and V.D.N.; funding acquisition, J.d.N., J.K., B.A.E., and P.V.-W.; investigation, A.P.-B., J.d.N., H.M., J.K., S.D., and S.A.; methodology, J.d.N., J.K., and P.V.-W.; project administration, J.d.N.; resources, J.d.N., J.K., and B.A.E.; supervision, J.d.N., J.K., B.A.E., and P.V.-W.; validation, J.K. and S.D.; visualization, J.d.N., A.P.-B., and V.D.N.; writing – original draft, J.d.N.; writing – review & editing, J.d.N., A.P.-B., P.V.-W., J.K., and B.A.E.

DECLARATION OF INTERESTS

The authors declare no competing interests.

STAR★METHODS

Detailed methods are provided in the online version of this paper and include the following:

- KEY RESOURCES TABLE
- EXPERIMENTAL MODEL AND STUDY PARTICIPANT DETAILS
- METHOD DETAILS
  - Transgene and clonal induction
  - Immunohistofluorescence
  - Cell counts
  - RNA-seq
  - RNA-seq and scRNA-seq analysis
  - Quantification of Delta expression
  - Segmentation and quantification in $Pros^+$ cells
  - Segmentation and quantification in Dl^+ cells
- QUANTIFICATION AND STATISTICAL ANALYSIS

SUPPLEMENTAL INFORMATION

Supplemental information can be found online at https://doi.org/10.1016/j.celrep.2025.115398.

Received: September 19, 2023
Revised: February 4, 2025
Accepted: February 14, 2025
Published: March 14, 2025

REFERENCES

1. Graf, T., and Enver, T. (2009). Forcing cells to change lineages. Forcing cells to change lineages *462*, 587–594. https://doi.org/10.1038/nature08533.
2. Levine, M., and Davidson, E.H. (2005). Gene regulatory networks for development. Proc. Natl. Acad. Sci. USA *102*, 4936–4942. https://doi.org/10.1073/pnas.0408031102.
3. Moris, N., Pina, C., and Arias, A.M. (2016). Transition states and cell fate decisions in epigenetic landscapes. Nat. Rev. Genet. *17*, 693–703. https://doi.org/10.1038/nrg.2016.98.
4. Simon, C.S., Hadjantonakis, A.-K., and Schröter, C. (2018). Making lineage decisions with biological noise: Lessons from the early mouse embryo. Wiley Interdiscip. Rev. Dev. Biol. *7*, 3199. https://doi.org/10.1002/wdev.319.

5. Cinquin, O., and Demongeot, J. (2005). High-dimensional switches and the modelling of cellular differentiation. J. Theor. Biol. *233*, 391–411. https://doi.org/10.1016/j.jtbi.2004.10.027.

6. Cinquin, O., and Demongeot, J. (2002). Positive and negative feedback: Striking a balance between necessary antagonists. J. Theor. Biol. *216*, 229–241. https://doi.org/10.1006/jtbi.2002.2544.

7. Crosnier, C., Stamataki, D., and Lewis, J. (2006). Organizing cell renewal in the intestine: stem cells, signals and combinatorial control. Nat. Rev. Genet. *7*, 349–359. https://doi.org/10.1038/nrg1840.

8. Jiang, H., and Edgar, B.A. (2012). Intestinal stem cell function in *Drosophila* and mice. Curr. Opin. Genet. Dev. *22*, 354–360. https://doi.org/10.1016/j.gde.2012.04.002.

9. Philpott, A., and Winton, D.J. (2014). Lineage selection and plasticity in the intestinal crypt. Curr. Opin. Cell Biol. *31*, 39–45. https://doi.org/10.1016/j.ceb.2014.07.002.

10. Micchelli, C.A., and Perrimon, N. (2006). Evidence that stem cells reside in the adult *Drosophila* midgut epithelium. Nature *439*, 475–479. https://doi.org/10.1038/nature04371.

11. Ohlstein, B., and Spradling, A. (2006). The adult *Drosophila* posterior midgut is maintained by pluripotent. Stem Cell. *439*, 470–474. https://doi.org/10.1038/nature04333.

12. Buchon, N., OSMAN, D., David, F.P.A., Fang, H.Y., Boquete, J.-P., Deplancke, B., and Lemaitre, B. (2013). Morphological and molecular characterization of adult midgut compartmentalization in *Drosophila*. Cell Rep. *3*, 1725–1738. https://doi.org/10.1016/j.celrep.2013.04.001.

13. Marianes, A., and Spradling, A.C. (2013). Physiological and stem cell compartmentalization within the *Drosophila* midgut. Elife *2*, e00886. https://doi.org/10.7554/elife.00886.015.

14. Bardin, A.J., Perdigoto, C.N., Southall, T.D., Brand, A.H., and Schweisguth, F. (2010). Transcriptional control of stem cell maintenance in the *Drosophila* intestine. Development *137*, 705–714. https://doi.org/10.1242/dev.039404.

15. Chen, J., Xu, N., Wang, C., Huang, P., Huang, H., Jin, Z., Yu, Z., Cai, T., Jiao, R., and Xi, R. (2018). Transient Scute activation via a self-stimulatory loop directs enteroendocrine cell pair specification from self-renewing intestinal stem cells. Nat. Cell Biol. *20*, 152–161. https://doi.org/10.1038/s41556-017-0020-0.

16. Zeng, X., and Hou, S.X. (2015). Enteroendocrine cells are generated from stem cells through a distinct progenitor in the adult *Drosophila* posterior midgut. Development *142*, 644–653. https://doi.org/10.1242/dev.113357.

17. Gervais, L., and Bardin, A.J. (2017). Tissue homeostasis and aging: new insight from the fly intestine. Curr. Opin. Cell Biol. *48*, 97–105. https://doi.org/10.1016/j.ceb.2017.06.005.

18. Perdigoto, C.N., Schweisguth, F., and Bardin, A.J. (2011). Distinct levels of Notch activity for commitment and terminal differentiation of stem cells in the adult fly intestine. Development *138*, 4585–4595. https://doi.org/10.1242/dev.065292.

19. Bertrand, N., Castro, D.S., and Guillemot, F. (2002). Proneural genes and the specification of neural cell types. Nat. Rev. Neurosci. *3*, 517–530. https://doi.org/10.1038/nrn874.

20. Murre, C. (2005). Helix-loop-helix proteins and lymphocyte development. Nat. Immunol. *6*, 1079–1086. https://doi.org/10.1038/ni1260.

21. Murre, C., Bain, G., VANDIJK, M.A., Engel, I., Furnari, B.A., Massari, M.E., Matthews, J.R., Quong, M.W., Rivera, R.R., and Stuiver, M.H. (1994). Structure and Function of Helix-Loop-Helix Proteins. Biochim. Biophys. Acta *1218*, 129–135. https://doi.org/10.1016/0167-4781(94)90001-9.

22. Massari, M.E., and Murre, C. (2000). Helix-loop-helix proteins: regulators of transcription in eucaryotic organisms. Mol. Cell Biol. *20*, 429–440.

23. Cabrera, C.V., and Alonso, M.C. (1991). Transcriptional activation by heterodimers of the achaete-scute and daughterless gene products of *Drosophila*. EMBO J. *10*, 2965–2973.

24. Cabrera, C.V., Alonso, M.C., and Huikeshoven, H. (1994). Regulation of scute function by extramacrochaete in vitro and in vivo. Development *120*, 3595–3603.

25. Van Doren, M., Ellis, H.M., and Posakony, J.W. (1991). The *Drosophila* extramacrochaetae protein antagonizes sequence-specific DNA binding by daughterless/achaete-scute protein complexes. Development *113*, 245–255.

26. Hartenstein, V., Takashima, S., Hartenstein, P., Asanad, S., and Asanad, K. (2017). bHLH proneural genes as cell fate determinants of entero-endocrine cells, an evolutionarily conserved lineage sharing a common root with sensory neurons. Dev. Biol. *431*, 36–47. https://doi.org/10.1016/j.ydbio.2017.07.013.

27. Amcheslavsky, A., Song, W., Li, Q., Nie, Y., Bragatto, I., Ferrandon, D., Perrimon, N., and Ip, Y.T. (2014). Enteroendocrine Cells Support Intestinal Stem-Cell- Mediated Homeostasis in *Drosophila*. Cell Rep. *9*, 32–39. https://doi.org/10.1016/j.celrep.2014.08.052.

28. Guo, Z., and Ohlstein, B. (2015). Bidirectional Notch signaling regulates *Drosophila* intestinal stem cell multipotency. Science *350*, aab0988, aab0988–aab0988. https://doi.org/10.1126/science.aab0988.

29. Beebe, K., Park, D., Taghert, P.H., and Micchelli, C.A. (2015). The *Drosophila* Prosecretory Transcription Factor dimmed Is Dynamically Regulated in Adult Enteroendocrine Cells and Protects Against Gram-Negative Infection. G3 (Bethesda, Md.) *5*, 1517–1524. https://doi.org/10.1534/g3.115.019117.

30. Lee, T., and Luo, L. (1999). Mosaic analysis with a repressible cell marker for studies of gene function in neuronal morphogenesis. Neuron *22*, 451–461.

31. Jiang, H., Patel, P.H., Kohlmaier, A., Grenley, M.O., McEwen, D.G., and Edgar, B.A. (2009). Cytokine/Jak/Stat signaling mediates regeneration and homeostasis in the *Drosophila* midgut. Cell *137*, 1343–1355. https://doi.org/10.1016/j.cell.2009.05.014.

32. Wang, L.-H., and Baker, N.E. (2015). E Proteins and ID Proteins: Helix-Loop-Helix Partners in Development and Disease. Dev. Cell *35*, 269–280. https://doi.org/10.1016/j.devcel.2015.10.019.

33. Tanaka-Matakatsu, M., Miller, J., Borger, D., Tang, W.-J., and Du, W. (2014). Daughterless homodimer synergizes with Eyeless to induce Atonal expression and retinal neuron differentiation. Dev. Biol. *392*, 256–265. https://doi.org/10.1016/j.ydbio.2014.05.019.

34. Li, Y., Pang, Z., Huang, H., Wang, C., Cai, T., and Xi, R. (2017). Transcription Factor Antagonism Controls Enteroendocrine Cell Specification from Intestinal Stem Cells. Sci. Rep. *7*, 988. https://doi.org/10.1038/s41598-017-01138-z.

35. Subramanian, A., Tamayo, P., Mootha, V.K., Mukherjee, S., Ebert, B.L., Gillette, M.A., Paulovich, A., Pomeroy, S.L., Golub, T.R., Lander, E.S., and Mesirov, J.P. (2005). Gene set enrichment analysis: A knowledge-based approach for interpreting genome-wide expression profiles. Proc. Natl. Acad. Sci. USA *102*, 15545–15550. https://doi.org/10.1073/pnas.0506580102.

36. Dutta, D., Dobson, A.J., Houtz, P.L., Gläßer, C., Revah, J., Korzelius, J., Patel, P.H., Edgar, B.A., and Buchon, N. (2015). Regional Cell-Specific Transcriptome Mapping Reveals Regulatory Complexity in the Adult *Drosophila* Midgut. Cell Rep. *12*, 346–358. https://doi.org/10.1016/j.celrep.2015.06.009.

37. Hung, R.-J., Hu, Y., Kirchner, R., Liu, Y., Xu, C., Comjean, A., Tattikota, S.G., Li, F., Song, W., Ho Sui, S., and Perrimon, N. (2020). A cell atlas of the adult *Drosophila* midgut. Proc. Natl. Acad. Sci. USA *117*, 1514–1523. https://doi.org/10.1073/pnas.1916820117.

38. Li, H., Janssens, J., De Waegeneer, M., Kolluru, S.S., Davie, K., Gardeux, V., Saelens, W., David, F.P.A., Brbić, M., Spanier, K., et al. (2022). Fly Cell Atlas: A single-nucleus transcriptomic atlas of the adult fruit fly. Science *375*, eabk2432. https://doi.org/10.1126/science.abk2432.

39. Lowe, N., Rees, J.S., Roote, J., Ryder, E., Armean, I.M., Johnson, G., Drummond, E., Spriggs, H., Drummond, J., Magbanua, J.P., et al.

(2014). Analysis of the expression patterns, subcellular localisations and interaction partners of *Drosophila* proteins using a pigP protein trap library. Development *141*, 3994–4005. https://doi.org/10.1242/dev.111054.

40. Lan, Q., Cao, M., Kollipara, R.K., Rosa, J.B., Kittler, R., and Jiang, H. (2018). FoxA transcription factor Fork head maintains the intestinal stem/progenitor cell identities in *Drosophila*. Dev. Biol. *433*, 324–343. https://doi.org/10.1016/j.ydbio.2017.09.002.
41. Doupé, D.P., Marshall, O.J., Dayton, H., Brand, A.H., and Perrimon, N. (2018). Drosophila intestinal stem and progenitor cells are major sources and regulators of homeostatic niche signals. Proc. Natl. Acad. Sci. USA *115*, 12218–12223. https://doi.org/10.1073/pnas.1719169115.
42. González, F., Romani, S., Cubas, P., Modolell, J., and Campuzano, S. (1989). Molecular analysis of the asense gene, a member of the achaete-scute complex of *Drosophila* melanogaster, and its novel role in optic lobe development. EMBO J. *8*, 3553–3562. https://doi.org/10.1002/j.1460-2075.1989.tb08527.x.
43. Patel, P.H., Dutta, D., and Edgar, B.A. (2015). Niche appropriation by *Drosophila* intestinal stem cell∼tumours. Nat. Cell Biol. *17*, 1182–1192. https://doi.org/10.1038/ncb3214.
44. Korzelius, J., Naumann, S.K., Loza-Coll, M.A., Chan, J.S., Dutta, D., Oberheim, J., Gläßer, C., Southall, T.D., Brand, A.H., Jones, D.L., and Edgar, B.A. (2014). Escargot maintains stemness and suppresses differentiation in *Drosophila* intestinal stem cells. EMBO J. *33*, 2967–2982. https://doi.org/10.15252/embj.201489072.
45. Loza-Coll, M.A., Southall, T.D., Sandall, S.L., Brand, A.H., and Jones, D.L. (2014). Regulation of *Drosophila* intestinal stem cell maintenance and differentiation by the transcription factor Escargot. EMBO J. *33*, 2983–2996. https://doi.org/10.15252/embj.201489050.
46. Furriols, M., and Bray, S. (2001). A model Notch response element detects Suppressor of Hairless-dependent molecular switch. Curr. Biol. *11*, 60–64.
47. Adam, J.C., and Montell, D.J. (2004). A role for extra macrochaetae downstream of Notch in follicle cell differentiation. Development *131*, 5971–5980. https://doi.org/10.1242/dev.01442.
48. Baonza, A., de Celis, J.F., and García-Bellido, A. (2000). Relationships between extramacrochaetae and Notch signalling in *Drosophila* wing development. Development *127*, 2383–2393.
49. Baonza, A., and Freeman, M. (2001). Notch signalling and the initiation of neural development in the *Drosophila* eye. Development *128*, 3889–3898.
50. Bhattacharya, A., and Baker, N.E. (2009). Developmental Biology. Dev. Biol. *327*, 288–300. https://doi.org/10.1016/j.ydbio.2008.11.037.
51. Spratford, C.M., and Kumar, J.P. (2015). Inhibition of Daughterless by Extramacrochaetae mediates Notch-induced cell proliferation. Development *142*, 2058–2068. https://doi.org/10.1242/dev.121855.
52. Puig-Barbé, A. (2019). A network of bHLH factors controls self-renewal and bipotential differentiation in the *Drosophila* intestine.
53. Bhattacharya, A., and Baker, N.E. (2011). A Network of Broadly Expressed HLH Genes Regulates Tissue-Specific Cell Fates. Cell *147*, 881–892. https://doi.org/10.1016/j.cell.2011.08.055.
54. Cubas, P., de Celis, J.F., Campuzano, S., and Modolell, J. (1991). Proneural clusters of achaete-scute expression and the generation of sensory organs in the *Drosophila* imaginal wing disc. Genes Dev. *5*, 996–1008.
55. Troost, T., Schneider, M., and Klein, T. (2015). A re-examination of the selection of the sensory organ precursor of the bristle sensilla of *Drosophila* melanogaster. PLoS Genet. *11*, e1004911. https://doi.org/10.1371/journal.pgen.1004911.
56. Li, K., and Baker, N.E. (2018). Regulation of the *Drosophila* ID protein Extra macrochaetae by proneural dimerization partners. Elife *7*, e33967. https://doi.org/10.7554/elife.33967.
57. van der Flier, L.G., van Gijn, M.E., Hatzis, P., Kujala, P., Haegebarth, A., Stange, D.E., Begthel, H., van den Born, M., Guryev, V., Oving, I., et al. (2009). Transcription factor achaete scute-like 2 controls intestinal stem cell fate. Cell *136*, 903–912. https://doi.org/10.1016/j.cell.2009.01.031.
58. Wice, B.M., and Gordon, J.I. (1998). Forced Expression of Id-1 in the Adult Mouse Small Intestinal Epithelium Is Associated with Development of Adenomas. J. Biol. Chem. *273*, 25310–25319. https://doi.org/10.1074/jbc.273.39.25310.
59. Zhang, N., Yantiss, R.K., Nam, H.S., Chin, Y., Zhou, X.K., Scherl, E.J., Bosworth, B.P., Subbaramaiah, K., Dannenberg, A.J., and Benezra, R. (2014). ID1 Is a Functional Marker for Intestinal Stem and Progenitor Cells Required for Normal Response to Injury. Stem Cell Rep. *3*, 716–724. https://doi.org/10.1016/j.stemcr.2014.09.012.
60. Andrade-Zapata, I., and Baonza, A. (2014). The bHLH Factors Extramacrochaetae and Daughterless Control Cell Cycle in *Drosophila* Imaginal Discs through the Transcriptional Regulation of the cdc25 Phosphatase string. PLoS Genet. *10*, e1004233. https://doi.org/10.1371/journal.pgen.1004233.
61. Wang, C., Guo, X., Dou, K., Chen, H., and Xi, R. (2015). Ttk69 acts as a master repressor of enteroendocrine cell specification in *Drosophila* intestinal stem cell lineages. Development *142*, 3321–3331. https://doi.org/10.1242/dev.123208.
62. Yin, C., and Xi, R. (2018). A Phyllopod-Mediated Feedback Loop Promotes Intestinal Stem Cell Enteroendocrine Commitment in *Drosophila*. Stem Cell Rep. *10*, 43–57. https://doi.org/10.1016/j.stemcr.2017.11.014.
63. Antonello, Z.A., Reiff, T., Ballesta-Illan, E., and Dominguez, M. (2015). Robust intestinal homeostasis relies on cellular plasticity in enteroblasts mediated by miR-8-Escargot switch. EMBO J. *34*, 2025–2041. https://doi.org/10.15252/embj.201591517.
64. Siudeja, K., Nassari, S., Gervais, L., Skorski, P., Lameiras, S., Stolfa, D., Zande, M., Bernard, V., Frio, T.R., and Bardin, A.J. (2015). Frequent Somatic Mutation in Adult Intestinal Stem Cells Drives Neoplasia and Genetic Mosaicism during Aging. Cell Stem Cell *17*, 663–674. https://doi.org/10.1016/j.stem.2015.09.016.
65. Zhai, Z., Kondo, S., Ha, N., Boquete, J.-P., Brunner, M., Ueda, R., and Lemaitre, B. (2015). Accumulation of differentiating intestinal stem cell progenies drives tumorigenesis. Nat. Commun. *6*, 10219–10227. https://doi.org/10.1038/ncomms10219.
66. Guo, X., Huang, H., Yang, Z., Cai, T., and Xi, R. (2019). Division of Labor: Roles of Groucho and CtBP in Notch-Mediated Lateral Inhibition that Controls Intestinal Stem Cell Differentiation in *Drosophila*. Stem Cell Rep. *12*, 1007–1023. https://doi.org/10.1016/j.stemcr.2019.03.005.
67. Korzelius, J., Azami, S., Ronnen-Oron, T., Koch, P., Baldauf, M., Meier, E., Rodriguez-Fernandez, I.A., Groth, M., Sousa-Victor, P., and Jasper, H. (2019). The WT1-like transcription factor Klumpfuss maintains lineage commitment of enterocyte progenitors in the *Drosophila* intestine. Nat. Commun. *10*, 4123. https://doi.org/10.1038/s41467-019-12003-0.
68. Tetteh, P.W., Basak, O., Farin, H.F., Wiebrands, K., Kretzschmar, K., Begthel, H., van den Born, M., Korving, J., de Sauvage, F., van Es, J.H., et al. (2016). Replacement of Lost Lgr5-Positive Stem Cells through Plasticity of Their Enterocyte-Lineage Daughters. Cell Stem Cell *18*, 203–213. https://doi.org/10.1016/j.stem.2016.01.001.
69. Diao, F., and White, B.H. (2012). A Novel Approach for Directing Transgene Expression in *Drosophila*: T2A-Gal4 In-Frame Fusion. Genetics *190*, 1139–1144.
70. Goldner, A.N., Fessehaye, S.M., Rodriguez, N., Mapes, K.A., Osterfield, M., and Doubrovinski, K. (2023). Evidence that tissue recoil in the early *Drosophila* embryo is a passive not active process. Mol. Biol. Cell *34*, br16. https://doi.org/10.1091/mbc.e22-09-0409.
71. Yesbolatova, A., Saito, Y., Kitamoto, N., Makino-Itou, H., Ajima, R., Nakano, R., Nakaoka, H., Fukui, K., Gamo, K., Tominari, Y., et al. (2020). The auxin-inducible degron 2 technology provides sharp degradation control in yeast, mammalian cells, and mice. Nat. Commun. *11*, 5701.
72. Vaessin, H., Grell, E., Wolff, E., Bier, E., Jan, L.Y., and Jan, Y.N. (1991). Prospero Is Expressed in Neuronal Precursors and Encodes a Nuclear-Protein That Is Involved in the Control of Axonal Outgrowth in *Drosophila*. Cell *67*, 941–953. https://doi.org/10.1016/0092-8674(91)90367-8.

73. Zeng, X., Chauhan, C., and Hou, S.X. (2010). Characterization of midgut stem cell- and enteroblast-specific Gal4 lines in *Drosophila*. Genesis *48*, 607–611. https://doi.org/10.1002/dvg.20661.

74. Presente, A., Shaw, S., Nye, J.S., and Andres, A.J. (2002). Transgene-mediated RNA interference defines a novel role for notch in chemosensory startle behavior. Genesis *34*, 165–169. https://doi.org/10.1002/gene.10149.

75. Schindelin, J., Arganda-Carreras, I., Frise, E., Kaynig, V., Longair, M., Pietzsch, T., Preibisch, S., Rueden, C., Saalfeld, S., Schmid, B., et al. (2012). Fiji: an open-source platform for biological-image analysis. Nat. Methods *9*, 676–682. https://doi.org/10.1038/nmeth.2019.

76. Dutta, D., Xiang, J., and Edgar, B.A. (2013). RNA Expression Profiling from FACS-Isolated Cells of the Drosophila Intestine. Curr. Protoc. Stem Cell Biol. *27*, 2F.2.1–2F.2.12. https://doi.org/10.1002/9780470151808.sc02f02s27.

77. Öztürk-Çolak, A., Marygold, S.J., Antonazzo, G., Attrill, H., Goutte-Gattat, D., Jenkins, V.K., Matthews, B.B., Millburn, G., Dos Santos, G., and Tabone, C.J.; FlyBase Consortium (2024). FlyBase: updates to the *Drosophila* genes and genomes database. Genetics *227*, iyad211. https://doi.org/10.1093/genetics/iyad211.

78. Barnett, D.W., Garrison, E.K., Quinlan, A.R., Strömberg, M.P., and Marth, G.T. (2011). BamTools: a C++ API and toolkit for analyzing and managing BAM files. Bioinformatics *27*, 1691–1692. https://doi.org/10.1093/bioinformatics/btr174.

79. Dobin, A., Davis, C.A., Schlesinger, F., Drenkow, J., Zaleski, C., Jha, S., Batut, P., Chaisson, M., and Gingeras, T.R. (2013). STAR: ultrafast universal RNA-seq aligner. Bioinformatics *29*, 15–21. https://doi.org/10.1093/bioinformatics/bts635.

80. Liao, Y., Smyth, G.K., and Shi, W. (2014). featureCounts: an efficient general purpose program for assigning sequence reads to genomic features. Bioinformatics *30*, 923–930. https://doi.org/10.1093/bioinformatics/btt656.

81. Love, M.I., Huber, W., and Anders, S. (2014). Moderated estimation of fold change and dispersion for RNA-seq data with DESeq2. Genome Biol. *15*, 550–621. https://doi.org/10.1186/s13059-014-0550-8.

82. Ritchie, M.E., Phipson, B., Wu, D., Hu, Y., Law, C.W., Shi, W., and Smyth, G.K. (2015). limma powers differential expression analyses for RNA-sequencing and microarray studies. Nucleic Acids Res. *43*, e47. https://doi.org/10.1093/nar/gkv007.

83. Korotkevich, G., Sukhov, V., Budin, N., Shpak, B., Artyomov, M.N., and Sergushichev, A. (2021). Fast gene set enrichment analysis. bioRxiv, 060012. https://doi.org/10.1101/060012.

84. Aibar, S., González-Blas, C.B., Moerman, T., Huynh-Thu, V.A., Imrichova, H., Hulselmans, G., Rambow, F., Marine, J.-C., Geurts, P., Aerts, J., et al. (2017). SCENIC: single-cell regulatory network inference and clustering. Nat. Methods *14*, 1083–1086. https://doi.org/10.1038/nmeth.4463.

85. Hu, Y., Comjean, A., Perkins, L.A., Perrimon, N., and Mohr, S.E. (2015). GLAD: an Online Database of Gene List Annotation for *Drosophila*. J. Genomics *3*, 75–81. https://doi.org/10.7150/jgen.12863.

86. Kanehisa, M., Furumichi, M., Sato, Y., Kawashima, M., and Ishiguro-Watanabe, M. (2023). KEGG for taxonomy-based analysis of pathways and genomes. Nucleic Acids Res. *51*, D587–D592. https://doi.org/10.1093/nar/gkac963.

87. Stuart, T., Butler, A., Hoffman, P., Hafemeister, C., Papalexi, E., Mauck, W.M., Hao, Y., Stoeckius, M., Smibert, P., and Satija, R. (2019). Comprehensive Integration of Single-Cell Data. Cell *177*, 1888–1902. https://doi.org/10.1016/j.cell.2019.05.031.

88. Hao, Y., Hao, S., Andersen-Nissen, E., Mauck, W.M., Zheng, S., Butler, A., Lee, M.J., Wilk, A.J., Darby, C., Zager, M., et al. (2021). Integrated analysis of multimodal single-cell data. Cell *184*, 3573–3587. https://doi.org/10.1016/j.cell.2021.04.048.

89. Street, K., Risso, D., Fletcher, R.B., Das, D., Ngai, J., Yosef, N., Purdom, E., and Dudoit, S. (2018). Slingshot: cell lineage and pseudotime inference for single-cell transcriptomics. BMC Genom. *19*, 477. https://doi.org/10.1186/s12864-018-4772-0.

90. Otsu, N. (1979). A threshold selection method from gray-level histograms. IEEE Transations on Systems, Man and Cybernetics *11*, 23–27.

91. Meyer, F., and Beucher, S. (1990). Morphological segmentation. J. Vis. Commun. Image Represent. *1*, 21–46. https://doi.org/10.1016/1047-3203(90)90014-m.

92. Li, C.H., and Lee, C.K. (1993). Minimum cross entropy thresholding. Pattern Recogn. *26*, 617–625. https://doi.org/10.1016/0031-3203(93)90115-d.

93. Heinze, G., Ploner, M., Jiricka, L., and Steiner, G. (2023). Firth's Bias-Reduced Logistic Regression. [R package logistf version 1.25] *1*, 33.

94. Albert, A., and Anderson, J.A. (1984). On the existence of maximum likelihood estimates in logistic regression models. Biometrika *71*, 1–10. https://doi.org/10.1093/biomet/71.1.1.

STAR★METHODS

KEY RESOURCES TABLE

REAGENT or RESOURCE	SOURCE	IDENTIFIER
Antibodies		
Mouse monoclonal anti-Delta, extracellular domain, c594.9b (1:50)	Developmental Studies Hybridoma Bank (DSHB)	RRID: AB_528194
Mouse monoclonal anti-Prospero, MR1A (1:200)	DSBH	RRID: AB_528440
Mouse monoclonal anti-Headcase, HDC U33 (1:100)	DSHB	RRID: AB_10659722
Mouse monoclonal anti-Armadillo, N2 7A1 (1:100)	DSHB	RRID: AB_528089
Rabbit polyclonal anti-Prospero (1:1000)	Vaessin et al.[72]	N/A
Guinea pig polyclonal anti-Emc (1:1000)	Antonio Baonza (CSIC, Spain)	N/A
Rabbit polyclonal anti-Phospho-Histone H3 (Ser10) (1:200)	Cell Signaling	Cat# 9701, RRID: AB_331535
Rabbit polyclonal anti-GFP (1:2000)	Abcam	Cat# ab6556, RRID: AB_305564
Chicken polyclonal anti-GFP (1:3000)	Abcam	Cat# ab13970, RRID: AB_300798
Chicken polyclonal anti-beta Galactosidase (1:2000)	Abcam	Cat# ab9361, RRID: AB_307210
Rabbit polyclonal anti-beta Galactosidase (1:10000)	ThermoFisher Scientific	Cat# A11132, RRID: AB_221539
Goat anti-Mouse IgG, Alexa Fluor 568-conjugated (1:500)	ThermoFisher Scientific	Cat# A-11031, RRID: AB_144696
Donkey anti-Mouse IgG, Alexa Fluor 594-conjugated (1:500)	ThermoFisher Scientific	Cat# A-21203, RRID: AB_2535789
Goat anti-Mouse IgG, Alexa Fluor 633-conjugated (1:500)	ThermoFisher Scientific	Cat# A-21050, RRID: AB_2535718
Goat anti-Rabbit IgG, Alexa Fluor 488-conjugated	ThermoFisher Scientific	Cat# A-11008, RRID: AB_143165
Donkey anti-Rabbit IgG, Alexa Fluor 594-conjugated	ThermoFisher Scientific	Cat# A-21207, RRID: AB_141637
Goat anti-Rabbit IgG, Alexa Fluor 633-conjugated	ThermoFisher Scientific	Cat# A-21070, RRID: AB_2535731
Goat anti-Guinea pig IgG, Alexa Fluor 546-conjugated	ThermoFisher Scientific	Cat# A-11074, RRID: AB_2534118
Goat anti-Chicken IgY, Alexa Fluor 488-conjugated	ThermoFisher Scientific	Cat# A-11039, RRID: AB_2534096
Goat anti-Chicken IgY, Alexa Fluor594-conjugated	ThermoFisher Scientific	Cat# A-11042, RRID: AB_2534099
Goat anti-Chicken IgY, Alexa Fluor 633-conjugated	ThermoFisher Scientific	Cat# A-21103, RRID: AB_2535756
Chemicals, peptides, and recombinant proteins		
Phosphate buffered saline tablets	Sigma-Aldrich	Cat# P4417
Triton X-100	Sigma-Aldrich	Cat# T8787
Bovine Serum Albumin fraction V	Roche	Cat# 10735108001
Formaldehyde solution	Sigma-Aldrich	Cat# F8775
Hoechst 33342 (used at 2 μg/mL)	Sigma-Aldrich	Cat# B2261
N-propyl-gallate	Sigma-Aldrich	Cat# 02370
Glycerol (spectrophotometric grade)	Sigma-Aldrich	Cat# G9012

(*Continued on next page*)

Continued

REAGENT or RESOURCE	SOURCE	IDENTIFIER
Critical commercial assays		
PureLink RNA mini preps	ThermoFisher Scientific	Cat# 12183020
Illumina polyA library preparation and NovaSeq PE sequencing	Genewiz/Azenta Life Sciences	N/A
Deposited data		
RNA-seq	This work	GEO:GSE234019
Single-cell RNA-seq	Hung et al.[37]	GEO:GSE120537
Single-cell RNA-seq	Li et al.[38]	ArrayExpress:E-MTAB-10519,ArrayExpress: E-MTAB-10628
Experimental models: Organisms/strains		
D. melanogaster: *Su(H)GBE-lacZ; esg-Gal4, UAS-GFP, tubP-Gal80^{ts}/CyO; UAS-FLP, Act5C-FRT-CD2-FRT-Gal4/TM6C* (*esg^{ts}-FO* driver)	Jiang et al.[31]	N/A
D. melanogaster: *y, w; Su(H)GBE-Gal4, UAS-GFP, tubP-Gal80^{ts}/CyO; UAS-FLP, Act5C-FRT-CD2-FRT-Gal4/TM6B* (*NRE^{ts}-FO* driver)	Zeng et al.[73]	Derived from RRID:BDSC_83377
D. melanogaster: *y, w; Su(H)GBE-Gal4/CyO; UAS-GFP, tubP-Gal80^{ts}/TM6B* (*NRE^{ts}* driver)	Zeng et al.[73]	Derived from RRID:BDSC_83377
D. melanogaster: *UAS-da*	Sonsoles Campuzano (CSIC, Spain)	N/A
D. melanogaster: *UAS-sc*	Sonsoles Campuzano	N/A
D. melanogaster: *emc^{EP3620}* (*UAS-emc* gene trap)	Sonsoles Campuzano	N/A
D. melanogaster: *UAS-p35*	Sonsoles Campuzano	N/A
D. melanogaster: *UAS-da:da*	Sangbin Park (Stanford University, USA)	N/A
D. melanogaster: *UAS-N^{ICD}*	Alfonso Martínez Arias (UPF, Spain)	N/A
D. melanogaster: *UAS-N^{RNAi}*	Presente et al.[74]	N/A
D. melanogaster: *UAS-H*	Allison Bardin (Curie Institute, France)	N/A
D. melanogaster: *UAS-esg*	Korzelius et al.[44]	N/A
D. melanogaster: *UAS-Dcr-2*	Bloomington *Drosophila* Stock Center (BDSC)	RRID:BDSC_24646
D. melanogaster: *y sc; UAS-da$^{RNAi}{}_{HMS01851}$*	BDSC	RRID:BDSC_38382
D. melanogaster: *y v;; UAS-da$^{RNAi}{}_{JF02488}$*	BDSC	RRID:BDSC_29326
D. melanogaster: *UAS-emc$^{RNAi}{}_{1007R-2}$*	National Institute of Genetics (Japan)	Stock# 1007R-2
D. melanogaster: *UAS-emc$^{RNAi}{}_{KK108316}$*	Vienna *Drosophila* Resource Center	Stock# 100587
D. melanogaster: *UAS-emc$^{RNAi}{}_{JF02300}$*	BDSC	RRID:BDSC_26738
D. melanogaster: *UAS-H$^{RNAi}{}_{JF02624}$*	BDSC	RRID:BDSC_27315
D. melanogaster: *UAS-esg$^{RNAi}{}_{HMS00025}$*	BDSC	RRID:BDSC_34063
D. melanogaster: *emc^{CPTI002740}*	Kyoto *Drosophila* Stock Center (DGRC)	Stock# 115317
D. melanogaster: *Myo1A-lacZ*	Jiang et al.[31]	RRID:BDSC_24646
D. melanogaster: *da-GFP.FPTB*	BDSC	RRID:BDSC_55836
D. melanogaster: *y w hs-Flp$_{1.22}$; Act5C-FRT-y^{+}-FRT-Gal4, UAS-lacZ$_{20b}$*	BDSC (modified)	RRID:BDSC_4410
D. melanogaster: *y w hs-Flp$_{1.22}$ tub-Gal4 UAS-GFP; tub-Gal80 FRT40A/CyO* (MARCM FRT40A)	Allison Bardin	N/A

(*Continued on next page*)

Continued

REAGENT or RESOURCE	SOURCE	IDENTIFIER
D. melanogaster: *y w hs-Flp$_{1.22}$ tub-Gal4 UAS-GFP; tub-Gal80 FRT80B/TM6B* (MARCM FRT80B)	Sonsoles Campuzano (Centro de Biología Molecular, Spain)	N/A
D. melanogaster: *y w hs-Flp$_{1.22}$ tub-Gal4 UAS-GFP; tub-Gal80 FRT2A/TM6B* (MARCM FRT2A)	Sonsoles Campuzano	N/A
D. melanogaster: *w hs-Flp tub-Gal80 FRT19A; tub-Gal4 UAS-GFP/CyO* (MARCM FRT19A)	Shinya Yamamoto (Baylor College, USA)	N/A
D. melanogaster: *w; FRT40A*	BDSC	RRID:BDSC_1646
D. melanogaster: *w;; FRT80B*	BDSC	RRID:BDSC_1620
D. melanogaster: *y w;; FRT2A*	BDSC	RRID:BDSC_1997
D. melanogaster: *y w FRT19A*	BDSC	RRID:BDSC_1709
D. melanogaster: *w; Df(2L)da^{10}, FRT40A/In(2LR)Gla, Bc*	BDSC	RRID:BDSC_5531
D. melanogaster: *w;; emc^{AP6} FRT80B/TM6B*	BDSC	RRID:BDSC_36544
D. melanogaster: *w;; emc^{1} FRT80B/TM2*	BDSC	RRID:BDSC_5532
D. melanogaster: *emc^{LL02590} FRT2A FRT82B/TM6C*	DGRC	Stock# 140642
D. melanogaster: *Df(1)sc^{B57} w FRT19A/FM7g*	Allison Bardin	N/A
Software and algorithms		
Rstudio	Posit Software PBC	http://www.rstudio.com
Illustrator CS6	Adobe Inc.	N/A
Photoshop CS6	Adobe Inc.	N/A
Affinity Designer 2	Serif (Europe) Ltd.	https://affinity.serif.com
FIJI	Schindelin et al.[75]	https://fiji.sc
Analysis scripts	this work	https://doi.org/10.5281/zenodo.8116966
Other		
Flygutseq	Dutta et al.[76]	https://flygutseq.buchonlab.com
Flybase	Öztürk-Çolak et al.[77]	https://flybase.org

EXPERIMENTAL MODEL AND STUDY PARTICIPANT DETAILS

Drosophila melanogaster experimental subjects were adult mated females, aged for ~2 weeks. Subject females were housed with males at a ratio of 1:2 to 3:4 males to females, to allow mating, at a density of 5–9 flies/**cm^2** of food surface and 2–3 flies/cm^3 of vial volume. Food was made from organic yellow maize flour (80 g/L), inactivated yeast powder (30 g/L), brewer's dextrose (80 g/L), agar (6.67 g/L), cooked at 95°C before adding propionic acid (0.5%) and tegosept (0.005%). Vials were kept at 18°C, 25°C or 29°C in a 12h:12h light/dark cycle. Breeding vials were flipped twice a week at 25°C and once at 18°C. Vials with adult experimental subjects were flipped every other day.

METHOD DETAILS

Transgene and clonal induction

For experiments using Gal80^{TS}, adult flies were aged to gut maturity (4–7 days) at 18°C, then transferred to 29°C. For induction of MARCM and flip-out clones, 4–7 days old flies were treated at 37°C for 60 or 15 min, respectively. Flies were aged for 7 days after induction treatment before dissection, unless otherwise indicated (see Table S2). Fly strains are listed in the key resources table. All RNAi transgenes were co-expressed with *UAS-Dcr-2*.

Immunohistofluorescence

For antibody staining, adult guts were dissected in ice-cold PBS (maximum 10 min). Tissues were fixed in PBS-formaldehyde 4% (15 min at room temperature, RT), then in methanol (15 min RT). Methanol was washed off with three rinses in PBS-Triton X100 0.1% (PBT), followed by blocking and permeabilisation in PBT-BSA 2% (PBTB; three times, 15 min each). Tissues were incubated overnight at RT in primary antibody solution (diluted in PBTB to their final concentration; see key resources table). Primary antibody was washed off with three rinses and three 15-min incubations in PBT at RT. Tissue was incubated in PBT-secondary antibody solution (2 h at RT), then rinsed three times and incubated twice in PBT (15 min each); then once more in PBS. Tissue was equilibrated in mounting medium (4:1 glycerol:PBS with 4% w/v N-propyl-gallate) 4 h at RT or overnight at 4°C. After mounting, 3D confocal imaging was performed in a Zeiss LSM 710 with an EC Plan-Neofluar 40X oil immersion objective (numerical aperture 1.3). Three fields of view (typically 213 μm × 213 μm) along the anterior-posterior axis of each of (at least) three posterior midguts (regions R4-R5)[12] were

imaged. In MARCM clone experiments, stacks were acquired from all clones found in each posterior midgut. Figures were assembled using FIJI and Adobe Photoshop/Illustrator CS6 or Affinity Designer 2.

Cell counts

For evaluating the proportion of cell types in GFP-labelled tissue, confocal stacks were maximum-intensity projected using FIJI and cells of the relevant types were counted manually with the Cell Counter plugin. Details of markers used can be found in Figure S1D. In the experiments co-expressing *sc* and *da:da*, the associated increase in proliferation generated large, highly densely populated cell clusters which could not be counted with single-cell precision. Therefore, for this genotype we estimated the proportion of each cell population in each field of view separately and then estimated the aggregated proportions.

RNA-seq

Flies bearing either *UAS-da*, *UAS-da*^{RNAi} (TRiP.JF02092), *UAS-da:da* or *UAS-sc* as well as *esg-Gal4*, *UAS-GFP* and *tub-Gal80*^{TS} were reared at 18°C until 4–7 days old, transferred to 29°C for 2 days and their midguts dissected, then processed as described.[76] Libraries from three biological replicates per condition (except one condition, with two) were prepared in two batches and ~37 million reads (either 50 or 300bp long, for each batch respectively) were generated per library using Illumina technology. See key resources table for additional details.

RNA-seq and scRNA-seq analysis

Fastq read files, with adaptors pre-trimmed by the sequencing provider, were mapped to release 6.28 of the *Drosophila melanogaster* genome using *STAR* and *bamtools*[78,79] and assigned to genes with *featureCounts*.[80] Differential gene expression, gene set and DNA motif enrichment analyses were performed with the key R packages *DEseq2*,[81] *limma*,[82] *fgsea*[83] and *RcisTarget*.[84] We performed GSEA[35] against the Gene List Annotation for *Drosophila* (GLAD),[85] the Kyoto Encyclopedia of Genes and Genomes (KEGG)[86] and gene lists from Dutta et al.[76] scRNAseq data were obtained from GEO and https://flycellatlas.org. To correct for variability arising from technical and biological effects, we used the *IntegrateData* function in *Seurat* v4.[87,88] The *Slingshot* library[89] was used for the trajectory analysis, which focused on ISC/EB cells as the initial state, pEC and EE cells, resulting in the identification of two distinct trajectories. The analysis code is in GitHub (https://github.com/jdenavascues/bHLH_code_midgut) and archived at Zenodo (https://doi.org/10.5281/zenodo.8116966).

Quantification of Delta expression

We took advantage of using simultaneously anti-Dl and anti-Pros mouse monoclonals, detected with the same anti-mouse secondary antibody, and of the robustness and reproducibility of the anti-Pros signal across conditions. This allows to use nuclear Pros staining outside the GFP-labelled MARCM clones as a normalisation reference, as the variation of Dl/Pros intensity ratio between samples is caused by the relative differences in Dl antigen. Dl$^+$ cells within clones and Pros$^+$ cells outside the clones were segmented so that we could take a value of fluorescence intensity per cell per marker, and normalised these values respect the average intensity of Pros per cell in that field of view.

Segmentation and quantification in Pros$^+$ cells

The positions of all cells were recorded in FIJI using CellCounter. A median filter was applied to the Pros/Dl channel to remove small features while preserving edges. A binary mask was created using Otsu thresholding[90] of the filtered image. This mask captured most of the Pros$^+$ nuclei but missed some with lower expression. To segment these, we used the manually determined XY positions of the Pros$^+$ cells to add a 3-pixel diameter disk for each Pros$^+$ cell absent in the original mask. Fused nuclei were separated by marker-controlled watershed transformation.[91] Pros expression for each nucleus was determined as the average pixel intensity value of the Pros signal channel in each segmented nucleus.

Segmentation and quantification in Dl$^+$ cells

Clones were detected by thresholding the GFP signal using the minimum cross-entropy method.[92] This missed a few cells, which were added to the mask using a similar approach to the Pros$^+$ nuclei, and the mask was consolidated by morphological filling and binary closing. Individual Dl$^+$ cells within the clone were identified by marker-controlled watershed segmentation, using the manually determined positions of the cells as markers. Dl expression for each cell was determined as the average pixel intensity of the Dl signal for each segmented object, normalised by the average Pros expression for that field of view.

QUANTIFICATION AND STATISTICAL ANALYSIS

Statistical tests were performed in R. Change in cell type composition was assessed by binomial logistic regression for each individual cell type. In experiments with zero observations in one cell type, we used Firth's bias-reduced logistic regression (package *logistf*)[93] to avoid the nonsensical results arising from the 'complete separation' of data.[94] All statistical tests and *p*-values of significance are specified in the corresponding figure legend; numbers of subjects are described either in the figure legend or Table S1 and Table S3. RNA-seq and scRNA-seq analyses are described in detail in their specific section and the code repository indicated there.